JOURNAL OF GEOPHYSICAL RESEARCH, VOL. 113, G01002, doi:10.1029/2007JG000438, 2008

An ecosystem model for tropical forest disturbance and selective logging

Maoyi Huang,[1] Gregory P. Asner,[1] Michael Keller,[2,3] and Joseph A. Berry[1]

Received 2 March 2007; revised 21 August 2007; accepted 6 September 2007; published 10 January 2008.

[1] A new three-dimensional version of the Carnegie-Ames-Stanford Approach (CASA) ecosystem model (CASA-3D) was developed to simulate regional carbon cycling in tropical forest ecosystems after disturbances such as logging. CASA-3D has the following new features: (1) an alternative approach for calculating absorbed photosynthetically active radiation (APAR) using new high-resolution satellite images of forest canopy gap fraction; (2) a pulse disturbance module to modify aboveground carbon pools following forest disturbance; (3) a regrowth module that simulates changes in community composition by considering gap phase regeneration; and (4) a radiative transfer module to simulate the dynamic three-dimensional light environment above the canopy and within gaps after forest disturbance. The model was calibrated with and tested against field observations from experimental logging plots in the Large-scale Biosphere Atmosphere Experiment in Amazonia (LBA) project. The sensitivity of key model parameters was evaluated using Monte Carlo simulations, and the uncertainties in simulated NPP and respiration associated with model parameters and meteorological variables were assessed. We found that selective logging causes changes in forest architecture and composition that result in a cascading set of impacts on the carbon cycling of rainforest ecosystems. Our model sensitivity and uncertainty analyses also highlight the paramount importance of measuring changes in canopy gap fraction from satellite data, as well as canopy light-use efficiency from ecophysiological measurements, to understand the role of forest disturbance on landscape and regional carbon cycling in tropical forests. In sum, our study suggests that CASA-3D may be suitable for regional-scale applications to assess the large-scale effects of selective logging, to provide guidance for forest management, and to understand the role of forest disturbance in regional and global climate studies.

Citation: Huang, M., G. P. Asner, M. Keller, and J. A. Berry (2008), An ecosystem model for tropical forest disturbance and selective logging, *J. Geophys. Res.*, *113*, G01002, doi:10.1029/2007JG000438.

1. Introduction

[2] Tropical forests have been threatened by increasing rates of forest degradation during the past 3 decades. Although deforestation, largely for the conversion of land to food crops or pastures, is the major destructive force in tropical forests worldwide [*Houghton et al.*, 2000], other forest disturbances such as the selective harvest of timber have also increased in frequency and extent [*Nepstad et al.*, 1999]. In selective logging, a limited number of marketable tree species are cut, and logs are transported off site to sawmills. Unlike deforestation, which is readily observed from satellites, selective logging in the Brazilian Amazon causes a spatially diffuse thinning of large trees, which is hard to monitor using satellite observations. Selective logging causes widespread collateral damage to remaining trees, subcanopy vegetation, and soils, with impacts on hydrological processes, soil erosion, fire, carbon storage, and plant and animal species.

[3] Recent remote sensing studies have made the monitoring of selective logging possible from the space. *Asner et al.* [2005a, 2006] developed a large-scale, high-resolution, automated remote-sensing analysis of selective logging and applied it to the top five timber-producing states of the Brazilian Amazon. Their results show that logging rates ranged from 12,075 to 19,823 km^2 per year (a) (±14%) between 1999 and 2002 in these states, equivalent to 60–123% of previously reported deforestation (forest clear-cut) area for those years.

[4] Current ecosystem models either operate at a broad spatial scale incompatible with diffuse forest disturbances such as selective logging, or at a very fine spatial scale that cannot easily ingest high-resolution data on forest canopy damage and disturbance over large geographic regions. The Ecosystem Demography (ED) model is an exception in that it is an individual-based terrestrial biosphere model which

[1]Department of Global Ecology, Carnegie Institution of Washington, Stanford, California, USA.
[2]USDA Forest Service, International Institute of Tropical Forestry, Rio Piedras, Puerto Rico.
[3]Complex Systems Research Center, University of New Hampshire, Durham, New Hampshire, USA.

0148-0227/08/2007JG000438$09.00

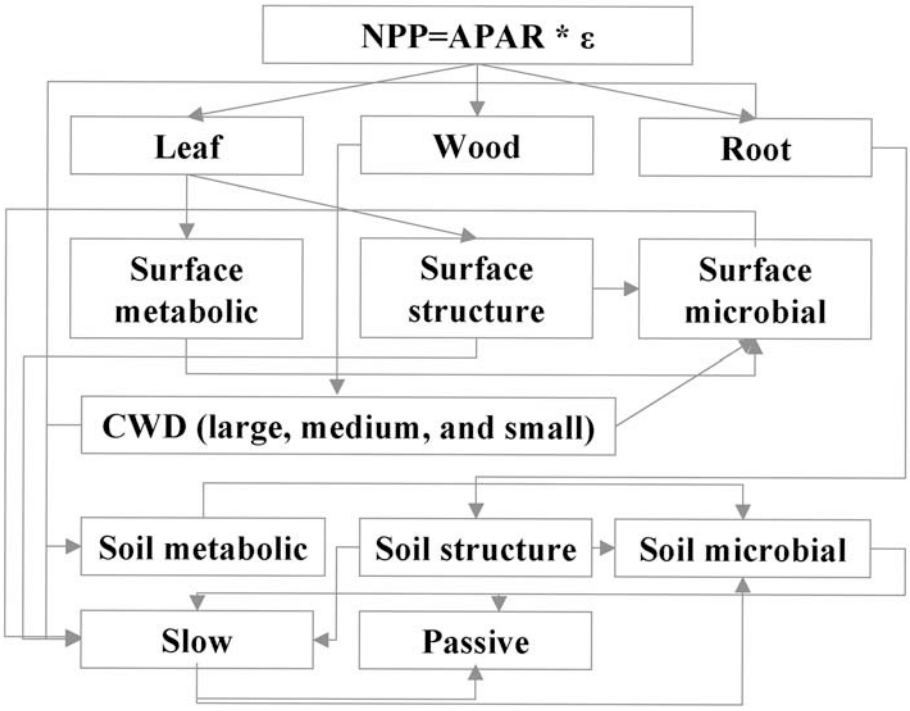

Figure 1. A schematic representation of the model structure of CASA. The boxes represent different carbon pools, and arrows represent the connections among the pools. CWD stands for the coarse woody debris pool.

can be scaled to large areas (e.g., a General Circulation Model (GCM) grid cell) with a size- and age-structured approximation [*Moorcroft et al.*, 2001]. However, it lacks an ability to simulate the carbon budget following disturbance such as selective logging. In the case of selective logging, an appropriate modeling approach is needed to simulate timber harvest impacts over large regions, meanwhile properly accounting for a necessary lack of site-specific information that is not expressed in remote sensing data (e.g., changes in forest community composition, light conditions, and stand structure after disturbance).

[5] To address these issues, we developed a new version of the Carnegie-Ames-Stanford Approach (CASA) ecosystem model (CASA-3D) designed specifically to quantify changes in carbon storage and fluxes following forest disturbance in humid tropical forests. The major new features of CASA-3D include: (1) an alternative way of estimating absorbed photosynthetically-active radiation (APAR) by taking advantage of new high-resolution satellite maps of forest canopy gap fraction [*Asner et al.*, 2005a]; (2) a pulse disturbance module to realistically modify carbon pools after forest disturbance; (3) a regrowth module that addresses changes in community composition following disturbance with a new set of parameterizations based on field observations of gap phase regeneration; and (4) a radiative transfer module for charactering the dynamic three-dimensional light environment above the canopy and within gaps after disturbance. This paper presents the novel combination of these new modules within CASA-3D and exercises the model on a well-measured tropical forest site in the central Amazon that was selectively logged during the Large-scale Biosphere-Atmosphere Experiment in Amazonia (LBA) program [*Keller et al.*, 2004a]. The new CASA-3D features are presented, followed by a calibration and testing carried out by comparison to data of net primary production (NPP), above ground biomass (AGB), coarse woody debris (CWD), net carbon exchange, and soil carbon pool collected at the Tapajos National Forest experimental logging sites [*Keller et al.*, 2004b; *Miller et al.*, 2004]. We then carry out a series of single-parameter and multiparameter sensitivity analyses to understand the absolute and relative importance of the major model parameters in describing and quantifying forest responses to selective logging. The uncertainties associated with the parameters are also discussed based on the sensitivity analyses.

2. Model Description

[6] The original CASA model was developed to simulate net primary production and carbon cycling in terrestrial ecosystems [*Potter et al.*, 1993a, 1993b; *Field et al.*, 1995]. The basic assumption of CASA is that for a given area, the amount of photosynthetically active radiation absorbed by green vegetation (APAR), multiplied by the light-use efficiency ε, equals NPP:

$$NPP = APAR \times \varepsilon \tag{1}$$

[7] The core structure of CASA is illustrated in Figure 1. In its original form, CASA estimates APAR as the product of solar surface irradiance and the fraction of photosynthetically active radiation absorbed by green vegetation (fPAR),

which can be estimated based on the Normalized Difference Vegetation Index (NDVI) from remote sensing products. The light-use efficiency (ε) for each grid cell is calculated as the product of a globally uniform maximum ε*, down-regulated by simulated water and temperature stress [*Field et al.*, 1995]. Carbon (C) that is fixed through NPP is then allocated into the live C stocks (e.g., leaf, wood, and root C pools), which are linked to the dead C pools (e.g., the surface coarse woody debris (CWD), soil, slow, and passive C pools) with different turnover rates [*Parton et al.*, 1989]. Respiration from the dead C pools is calculated based on specified decay rates of those pools, combined with mediating factors such as temperature and precipitation. In sum, CASA provides a straightforward means to estimate the NPP, respiration, net ecosystem production (NEP), and carbon stocks of an ecosystem [e.g., *Potter et al.*, 1993a, 1993b; *Randerson et al.*, 1997].

[8] Despite the success and general applicability of CASA to ecosystem C research at regional and global scales, a number of factors have limited its applicability to forest disturbance studies. First, the relatively low spatial resolution and high temporal resolution requirement of the NDVI inputs for the CASA NPP calculation, along with the assumption that the vegetation is homogeneous within a grid cell or image pixel, leaves CASA unable to account for noncontiguous (sporadic) changes in vegetation leaf area and fPAR that occur at fine spatial resolution. Second, the basic CASA formulation was designed to estimate C stocks and fluxes at equilibrium conditions, and thus it cannot capture dynamic changes in C cycle processes resulting from changes in forest architecture and composition following forest disturbance. We address these specific limitations in the following sections.

2.1. An Alternative Calculation of APAR

[9] CASA traditionally estimated fPAR and NPP based on time series of NDVI, usually from the NOAA Advanced Very High Resolution Radiometer (AVHRR) or Terra Moderate Resolution Imaging Spectrometer (MODIS) sensors with 250–1000 m spatial resolution. However, these satellite resolutions and methods do not resolve selective logging [*Asner et al.*, 2005a]. Even at a high spatial resolution, for example, 30-m Landsat Enhanced Thematic Mapper Plus (ETM+) satellite data, the NDVI only provides overall canopy greenness at each pixel and has very little information on the ecosystem structure [*Asner et al.*, 2002a].

[10] *Asner et al.* [2005a, 2006] developed the Carnegie Landsat Analysis System (CLAS) to study the forest structural attributes using Landsat ETM+ and TM data with automated subpixel analysis methods. The fractional cover of photosynthetic vegetation (PV), nonphotosynthetic vegetation (NPV), and bare substrate in each pixel is estimated with CLAS. These quantities capture the biophysical impacts of many types of disturbances, both natural (e.g., tree-fall gaps and larger blow-downs) and human-caused (e.g., logging). Pattern recognition algorithms are then used to distinguish selective logging from natural gaps. Extensive validation of the method showed that it could detect and map logging areas with absolute uncertainties of 11–14%. A detailed explanation of the algorithms is provided by *Asner et al.* [2005a]. *Asner et al.* [2005b, 2006] also showed that the PV fractional cover per pixel is related to forest canopy gap fraction. Taking this a step further for CASA-3D, we employ the basic principles reviewed by *Campbell and Norman* [1998] to simulate fPAR from remotely sensed gap fraction:

$$fPAR = 1 - gap \tag{2}$$

where "gap" is forest canopy gap fraction at a spatial resolution of 28.5 m by 28.5 m from Landsat 7. This simple modification to CASA provides the opportunity to incorporate the sporadic observations of forest gap fraction from Landsat, usually 1–2 times per year in the Amazon due to cloud cover [*Asner*, 2001], to modify the fPAR environment of a forest stand during recovery from disturbance.

2.2. A Pulse Disturbance Module

[11] The new pulse disturbance module of CASA-3D is designed to modify the C pools immediately following forest disturbance. For example, selective logging causes ground damage and tree mortality leading to fluxes from live into detrital C pools as a pulse after timber harvest [*Pereira et al.*, 2002; *Keller et al.*, 2004b]. These C fluxes are calculated as:

$$\begin{aligned} Cout_{\text{wood}} &= f_{\text{logged}} \times S_{\text{wood}} \\ Cout_{\text{leaf}} &= f_{\text{logged}} \times S_{\text{leaf}} \\ Cout_{\text{froot}} &= f_{\text{logged}} \times S_{\text{froot}} \end{aligned} \tag{3}$$

where *Cout* is the carbon taken out of the C pools due to logging, *S* represents the storage of C in a given pool before logging, and f_{logged} is the fraction of the canopy removed within each image pixel (from CLAS [*Asner et al.*, 2005b]). The formulation of equation (3) is based on the assumption that biomass loss is proportional to canopy loss in a pixel. Field evidence from Cauaxi, Brazil [*Pereira et al.*, 2002; *Keller et al.*, 2004b] showed that CWD mass is correlated with gap fraction with a slope of 281 Mg/ha, which is close to the estimated above ground biomass (AGB) at that site and an intercept of 45 Mg/ha nearly the total CWD in undisturbed forest. Because CWD constitutes the major portion of *Cout* [see *Asner et al.*, 2005a, Table S6], equation (3) is not only reasonable from a mass balance point of view but is also supported by field observations.

[12] $Cout_{\text{wood}}$ consists of two components: (1) the wood volume removed and transported off-site, and (2) the collateral biomass lost to coarse woody debris (CWD) and standing dead (SDD) pools. According to *Pereira et al.* [2002] and *Asner et al.* [2005a], gap fraction can be used to estimate the volume of roundwood (m^3/ha) extracted on a per-area basis using an equation drawn from 35 logging sites in Brazil, Belize, Suriname, Guyana, and Indonesia as:

$$Volume_{\text{wood}} = 3.882 + 108.7 \cdot gap \tag{4}$$

The amount of carbon (g C/ha) transported off-site then becomes:

$$C_{\text{offsite}} = 0.5 \cdot \rho_{\text{wood}} \cdot Volume_{\text{wood}} \tag{5}$$

where ρ_{wood} is the specific wood density.

[13] The necromass, including CWD and SDD, left on site is given as:

$$Necromass = Cout_{\text{wood}} - C_{\text{offsite}} \quad (6)$$

where the relationship between CWD and SDD in Mg/ha [*Palace et al.*, 2007] is characterized by:

$$CWD = 4.3 \cdot SDD + 18.6 \quad (7)$$

[14] In CASA-3D, CWD is divided into large, medium, and small pools based on *Keller et al.* [2004b] and *Palace et al.* [2007] to reflect the fact that the decay rates of various size classes of CWD are quite different, and, for decomposition calculations, SDD is treated as part of the large CWD pool. The partitioning of losses from the wood C pools to large, medium, and small CWD pools are 0.8818, 0.0798, and 0.0384 in the intact forest (unlogged) case, and 0.7813, 0.1395, and 0.0722 in the logged case, respectively [*Keller et al.*, 2004b; *Palace et al.*, 2007]. In addition, foliar losses (e.g., $Cout_{\text{leaf}}$) enter the surface metabolic and surface structural C pools, while fine root losses (i.e., $Cout_{\text{froot}}$) go to soil metabolic and soil structural pools, with the metabolic fraction determined by the *lignin:N* ratio at a specific site [*Potter et al.*, 1993a, 1993b].

2.3. A New Regrowth Module Considering Community Ecology

[15] Gap phase regeneration of trees has been a topic of ecosystem research and modeling for decades. Forest gap models [e.g., *Botkin et al.*, 1972; *Shugart*, 1984; *Bossel and Krieger*, 1991; *Bugmann*, 2001] are a group of individual-tree based, semimechanistic simulators designed to study tree population dynamics on small patches of land [*Risch et al.*, 2005]. These models require site- and species-specific information to facilitate interspecific competition for light, water, and nutrients but also capture the stochastic nature of tree establishment and mortality. *Alder and Silva* [2000] developed an empirical cohort model for management of Terra Firme forests in the Brazilian Amazon. Forest stands are represented by as many as 54 cohorts, each with their own parameters for diameter increment, mortality, and recruitment. None of these models is suitable for our purposes due to their complexity and requirement of detailed site- and/or species-specific information. Although *Moorcroft et al.* [2001] introduced a size- and age-structured (SAS) approximation to scale the ED model to broader geographic and/or temporal scales, the individual-based gap simulator in the ED model are based on assumptions that are not appropriate to be applied under a selective logging scenario. We therefore developed a forest regrowth module for CASA-3D that takes advantage of the remotely sensed gap fractions from Landsat to track the C budget with a small number of parameters as possible.

[16] The primary input to the regrowth module is the gap fraction of each pixel from satellite images at a resolution of 28.5 by 28.5 m, along with a postlogging forest recovery function based on *Asner et al.* [2006], which is given by:

$$gap(t) = \left(\alpha_0 + \alpha_1 \cdot t^2 + \alpha_2 \cdot t^{0.5}\right)^{-1} \quad (8)$$

where t is the number of years after logging, $gap(t)$ ($0 \leq gap(t) \leq 1$) is the averaged gap fraction of a pixel, and parameters α_0, α_1, and α_2 can be estimated as:

$$\alpha_0 = \left[-22.59 + 0.41 \cdot (gap_0 \times 10)^2 + 24.91 \cdot (gap_0 \times 10)^{0.5}\right]^{-1}$$

$$\alpha_1 = -0.00147 + 0.000116 \cdot (gap_0 \times 10) + 0.00346 / (gap_0 \times 10)$$

$$\alpha_2 = 0.00685 + [-0.0630 / \ln(gap_0 \times 10)] + 0.11388 / (gap_0 \times 10)^{0.5}$$

where gap_0 is the gap fraction immediately following timber harvest.

[17] Within each pixel, the forest is divided into two components: the intact fraction and the logged fraction. Assuming that canopy gap of the logged fraction immediately following harvest ($gap_{\text{logged}}(t = 0)$) is 1.0 (no canopy), the logged fraction of a given pixel can be calculated as:

$$f_{\text{logged}} = (gap_0 - gap_{\text{intact}}) / \left(gap_{\text{logged}}(t = 0) - gap_{\text{intact}}\right) \quad (9)$$

where gap_{intact} is the gap fraction of the intact forest, which is assumed to be the same as the gap fraction before logging. With equation (9), the gap fraction of the logged portion of the forest as a function of t is given by:

$$gap_{\text{logged}}(t) = \left[gap(t) - \left(1 - f_{\text{logged}}\right) \cdot gap_{\text{intact}}\right] / f_{\text{logged}} \quad (10)$$

[18] Equations (8)–(10) serve as an essential additional basis for the NPP calculation in CASA-3D. After logging, the NPP of the intact canopy and of the logged canopy are estimated based on gap_{intact} and gap_{logged}, respectively, with fPAR estimated using equation (2). The overall NPP of each pixel is then calculated by weighted-averaging of the NPP of the two forest components according to their fractions in the pixel.

2.3.1. Species Composition Within Logged Portion of the Canopy

[19] Species composition of the intact and logged portions of the forest are different [e.g., *Brokaw*, 1985, 1987; *Pinard and Cropper*, 2000; *Clark and Clark*, 1999; *Webb*, 1998]. The intact forest is dominated by shade tolerant species, while the logged portion of the forest is dominated by pioneer species in early stages with more shade tolerant forest species gradually becoming dominant. The gap phase regeneration has significant impacts on forest architecture, composition, tree population dynamics, and the C budget. To capture these effects, we divide the gap species into three functional types:

[20] 1. Pioneer species are species that colonize gaps from seeds which are typically light-demanding and which grow rapidly in the early stage of forest regeneration [*Brokaw*, 1985, 1987]. An important feature of pioneer species is that they need full light for both germination and seedling establishment, and their seedlings are not often found in deep canopy shade [*Whitemore*, 1998]. *Cecropia* is a good example of a forest pioneer genus.

[21] 2. Light-demanding primary species are those that can germinate in deep shade and have seedlings that die

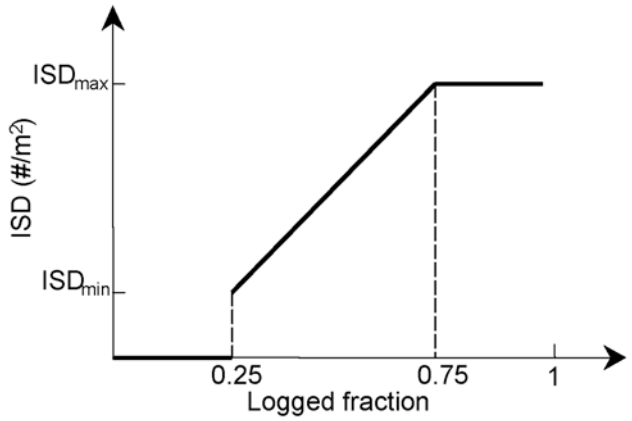

Figure 2. Initial stand density of pioneer species in a gap as a function of gap fraction.

unless they get full light within about a year; they normally grow fast with pale and soft timbers [*Whitemore*, 1998].

[22] 3. Shade tolerant primary species are species that can germinate, establish, and remain alive even under consistent deep shade; they normally grow slowly with dark and dense timbers [*Whitemore*, 1998].

[23] With this classification scheme in CASA-3D, different sets of regrowth parameters/parameterizations are assigned to different functional types. The parameters include maximum light-use efficiency (ε^*), specific wood density, stem density, and tree allometrics. We note that although most studies of gap dynamics were based on observations in natural gaps, the dynamics were not fundamentally different between natural and logging gaps, especially when the species were categorized into a few functional types [*Whitemore*, 1998]. For example, *Webb* [1998] showed that the community dynamics in selectively logged lowland forest in Costa Rica were similar to that of naturally disturbed forests.

[24] *Whitemore* [1998] pointed out that there exists a threshold of gap size for establishment of pioneer species. In lowland tropical forests, pioneers are commonly observed in gaps above about 200 m^2 in size. Field data on regeneration in 30 gaps ranging in size from 20 to 705 m^2 in tropical forest on Barro Colorado Island (BCI), Panama also show that the threshold is ~200 m^2 [*Brokaw*, 1985]. In forests places with lower temperature and/or humidity, the threshold might be higher. In this initial study with CASA-3D, the threshold is represented in terms of gap fraction. When the gap fraction of a satellite pixel is larger than 25% (or 203 m^2), pioneer species are simulated in the regrowth of the forest canopy in that pixel. Otherwise, only primary species are simulated. Also, according to *Brokaw* [1985, 1987], the initial established stem density of pioneer species in 1 year (a) after logging is correlated with the gap size as:

$$ISD_{\text{pioneer}} = \begin{cases} 0, & f_{\text{logged}} < gap_{th} \\ ISD_{\min} + \dfrac{ISD_{\max} - ISD_{\min}}{0.75 - gap_{th}} * \left(f_{\text{logged}} - gap_{th}\right), & \text{where } gap_{th} \le f_{\text{logged}} < 0.75 \\ ISD_{\max}, & f_{\text{logged}} \ge 0.75 \end{cases}$$

where ISD$_{\min}$ and ISD$_{\max}$ are parameters defining the maximum and minimum possible initial established stem density of pioneers in the first year of regrowth within a gap. This relationship is illustrated in Figure 2, showing the stem density/gap fraction curve that we use to define the initial stem density of pioneer species in each pixel. In this initial study, $ISD_{\min}$ = 50 stems/ha and $ISD_{\max}$ = 300 stems/ha, also based on *Brokaw* [1985, 1987].

[25] Field studies show that the stem density of established pioneer species varies. For example, if *Cecropia* is the major pioneer species established, its stem density would be the highest in the first year and would decrease exponentially after that. For other pioneers, the stem density remains stable or even increases during the first few years and starts to decrease exponentially thereafter. According to *Silva et al.* [1995], the only pioneer genus in the Tapajos field sites where we are working is *Cecropia*. *Brokaw* [1987] showed that the stem density of *Cecropia* as a function of time t (in years) after gap formation could be estimated as:

$$SD(t) = \begin{cases} ISD_{\text{pioneer}} \cdot t^{-0.6592}, & t \ge 1 \\ ISD_{\text{pioneer}} \cdot t, & t \le 1 \end{cases} \tag{11}$$

where ISD_{pioneer} is the stem density of pioneer species one year after logging in each pixel (Figure 2). Figure 3 shows the relation between the stem density of pioneer species and number of years after gap formations as given by equation (11). Note that the turnover time of the pioneer C pool ranges from 6 to 14 years, which is much shorter than that of primary species.

[26] Different from that of the pioneer species, the stem density of the established primary species (both light-demanding and shade-tolerant types) is assumed to increase linearly from SD$_0$ to SD$_1$ in the first few years and remains stable thereafter [*Brokaw*, 1987]. Parameters $T_{\text{p\_ld}}$ and $T_{\text{p\_st}}$ are introduced to represent the time for light-demanding species and shade-tolerant species to reach their maximum stem densities SD$_{1_\text{ld}}$ and SD$_{1_\text{st}}$, respectively.

[27] The self-thinning process of the primary species is simulated by assuming that only the first group of trees entering into the 2 cm diameter at the breast height (DBH) class will eventually succeed in reaching the upper canopy [*Molino and Sabatier*, 2001]. Late recruits will remain in the shade and grow slowly, especially among the shade-tolerant primary species. In CASA-3D, the final stem density of primary species typically ranges from 500 to 600 per ha across all gap sizes. Successful individuals continue to grow based on allometric relationships described later.

[28] With the above parameterizations, the partitioning of NPP from equation (10) among the three functional types of gap species is based on the ratio of their stem densities with

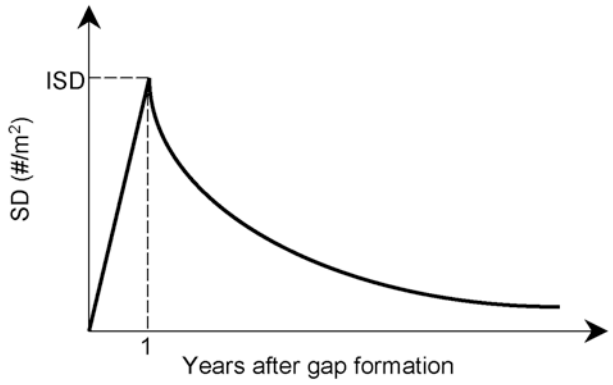

Figure 3. Stem density of pioneer species as a function of time after gap formation.

respect to the overall stem density in the gap at time *t*. In the two primary species functional types, we partition NPP further into two size classes:

[29] 1. The first class is potential canopy trees with a turnover period of $wood_{age}$ years.

[30] 2. For the understory shade-tolerant species, a turnover period of $ST\_understory_{age}$ (up to 100 years) [*Vieira et al.*, 2005] is used for this class because the shade-tolerant trees can remain in the shade for a long period, maintaining very slow growth rate. For understory light-demanding species, a turnover period of $LD\_understory_{age}$ (~25 years) reflects the fact that those trees cannot persist in the shade. The allocation of NPP between the potential canopy trees and slow-growing understory trees is based on the assumption that the contribution of understory trees to the total NPP decreases from a percentage of $f_{understory}$% to 0% in a period of $T_{understory}$ years.

2.3.2. Allometric Equations

[31] Two sets of allometric equations are used to simulate the regrowth of pioneer and primary functional types, respectively. *Chave et al.* [2005] suggest that aboveground biomass (AGB) of a tree in the tropical forest can be related to its diameter at breast height (DBH) as:

$$AGB = \rho_{wood} * \exp\{a_0 + a_1 \cdot \ln(DBH) + a_2 \cdot [\ln(DBH)]^2 + a_3 \cdot [\ln(DBH)]^3\} \quad (12)$$

where ρ_{wood} is the specific wood density, a_0, a_1, a_2, and a_3 are parameters determined based on field data. For our purposes, the height (H) of trees can be estimated based on a H-DBH relationship [*Keller et al.*, 2001] as:

$$H = \begin{cases} c_1 \cdot DBH^{c_2}, & DBH \geq 10\,\text{cm} \\ c_3 \cdot DBH, & DBH \leq 10\,\text{cm} \end{cases} \quad (13)$$

where c_1 and c_2 were estimated from field data and $c_3 = (c_1 \cdot 10^{c_2})/10$, following *King* [2005]. Equation (12) is used to simulate the regrowth of the primary species with parameters given by *Chave et al.* [2005].

[32] The allometric equation for the pioneer functional type is taken from *Nelson et al.* [1999], which was developed in secondary forests in central Amazon. As discussed above, *Cecropia* is the major pioneer genus and its allometric equation is given by:

$$\ln(AGB) = a_4 + a_5 \ln(DBH) \quad (14)$$

where a_4 and a_5 equal −2.5118 and 2.4257, respectively, according to *Nelson et al.* [1999]. *Sposito and Santos* [2001] studied eight *Cecropia* species in Amazonian and southeastern forests of Brazil. They suggested that the H-DBH relationship for *Cecropia* in forest gap understory could be estimated as:

$$\log_{10} H = (\log_{10} DBH + 0.0130)/1.024 \quad (15)$$

2.4. Radiative Transfer Module

[33] After logging, more light penetrates and reaches the understory of the forest. Competition among gap species for light is an essential factor determining their photosynthesis and regrowth rates [*Denslow*, 1987]. To provide a realistic simulation of the dynamic light environment, we separate the incoming solar radiation into direct and diffuse components. For the intact forest, our partitioning of solar radiation is used to modify photosynthetic capacity via dynamic changes in light-use efficiency. For the regrowing forest, a canopy geometric-optic (GOMS) submodel is employed to simulate three-dimensional (3-D) shadowing within gaps generated by beam radiation; diffuse radiation is further partitioned into direct and indirect diffuse components, which are transmitted through different pathways into the gaps.

2.4.1. Separation of Incoming Solar Radiation Above Canopy

[34] The partitioning of incoming radiation into direct beam and diffuse components (e.g., R_{beam} and R_{diff}) has a significant impact on photosynthesis by way of inherent physiological responses of plants to light [*Spitters et al.*, 1986]. In CASA-3D, equation (9) from *Spitters et al.* [1986] is employed for separating R_{diff} and R_{beam} above the canopy. This equation is based on the ratio between measured daily irradiance at the Earth surface and the estimated exoatmospheric radiation. Within a pixel, the transmission of radiation is treated differently for intact and logged portions of the forest canopy. For the intact portion, the fraction of incoming radiation that penetrates to the forest floor is small and the growth of understory trees is negligible. Therefore we treat the intact forest as a one-layer system without considering the 3-D shadowing of beam radiation and transfer of diffuse radiation into the forest floor. According to *Anderson et al.* [2000], under different illumination conditions, the light-use efficiency of plants varies with the fraction of diffuse radiation as:

$$\varepsilon' = \varepsilon \cdot [1 + 2 \cdot \Delta_{diff}(f_{diff} - 0.5)] \quad (16)$$

where f_{diff} is the fraction of diffuse radiation, ε is the light-use efficiency under the condition that $f_{diff} = 0.5$. Δ_{diff} equals 0.4 for C3 plants and 0.15 for C4 plants. Furthermore, $f_{diff} = R_{diff}/(R_{beam} + R_{diff})$ is used for the area of sunlit crowns and $f_{diff} = 1$ for the area of shaded crowns

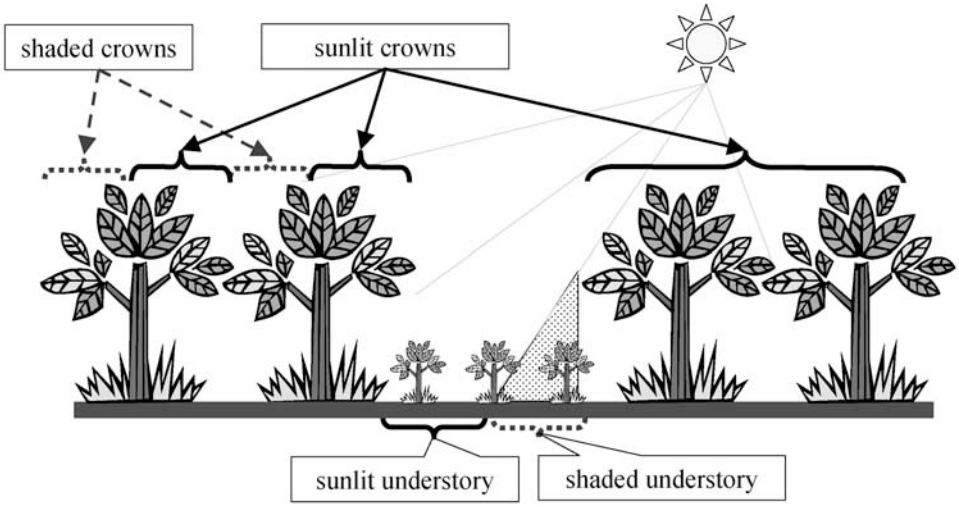

Figure 4. A schematic representation of the three-dimensional shadowing module for simulating the transmission of direct beam radiation within gaps.

because only diffuse radiation can reach the shaded portion of a crown. Fractions of sunlit and shaded crowns are estimated with the GOMS 3-D shadowing model described below.

2.4.2. 3-D Shadowing of Beam Radiation in Gaps

[35] The transmission of R_{beam} is represented with a 3-D shadowing module comprised of a canopy geometric-optic (GOMS) model [*Li and Strahler*, 1992; *Asner et al.*, 1998], and as shown in Figure 4. This module provides quantitative data on fractions of sunlit understory, sunlit crowns, and total shaded area at each time step. It requires solar angles as inputs and parameters to describe forest geometry. Detailed discussions of the GOMS approach, and its parameters, can be found in the work of *Li and Strahler* [1992], *Abuelgasim and Strahler* [1994], and *Asner et al.* [1998]. The GOMS parameters used in CASA-3D are listed in Appendix A.

[36] In this study, GOMS is coupled to the regrowth module. As shown in Figure 4, in order to simulate the light environment within gaps, the following parameters need to be specified: (1) The density of intact crowns per pixel λ, which is estimated with the averaged gap fraction of the pixel as $(1 - gap(0))/(\pi r^2)$; (2) The average crown radius r, half height of the tree crown b, and crown vertical-to-horizontal diameter ratio *brratio* of the intact trees within the pixel, which are estimated based on statistics taken from field data collected in the eastern Amazon [*Asner et al.*, 2002b]. The coupling of GOMS and the regrowth module is established through the parameters h_{diff} and *hbratio*, which are the height of canopy from understory to crown center and the ratio between h_{diff} and b (*hbratio*), respectively. We treat the forest within a pixel as a two-layer system. One layer is the intact forest and the other is the regrowing trees within gaps. Then, $h_{\text{diff}} = h - h_{\text{rg}}$ is the height of canopy from the top of the understory to crown center, where h is the average height of the intact trees, and h_{rg} is the average height of the regrowing trees simulated by the regrowth module.

[37] The solar zenith and azimuth angles are the drivers of GOMS. Those angles change with the position of sun at a given study site. To capture the diurnal and seasonal changes in solar position, a monthly mean diurnal cycle of solar angles at a 30-min temporal resolution for each month is embedded in the model so that the diurnal and seasonal cycles of fractions of sunlit understory, sunlit crowns and shaded area can be accurately represented for any point on Earth. As a consequence, NPP is also calculated and allocated to the C pools according to those cycles.

2.4.3. Transmission of Diffuse Radiation in Gaps

[38] In principle, diffuse radiation can be treated as multiple beams from all directions of the sky and a diffuse transmission coefficient for the canopy can be calculated from:

$$\tau_d = 2\int_{x_1}^{x_2} G \cdot \sin\psi \cdot \cos\psi \cdot d\psi \tag{17}$$

where G is the fraction of incident radiation from zenith angle ψ that penetrates the canopy, x_1 and x_2 are the zenith angles of interest for integrating the incident radiation. For a heterogeneous (gap) canopy, the transmission coefficient for the direct diffuse radiation (R_{dd}, the diffuse radiation transmitted through the top of the gap) is given by:

$$\begin{aligned}\tau_{dd} &= 2\int_0^{\theta} \sin\psi \cdot \cos\psi \cdot d\psi = 2\int_{\sin 0}^{\sin\theta} \sin\psi d\sin\psi \\ &= 2\cdot\left(\frac{\sin^2\theta}{2} - 0\right) = \sin^2\theta\end{aligned} \tag{18}$$

where θ is the zenith angle corresponding to the gap opening as shown in the Figure 5, and G = 1 in this case because there are no obstacles in the pathway of transmission. Note that by using equation (18), we assume that each gap is circular in shape and that the distribution of diffuse radiation is uniform. The transmission coefficient for the

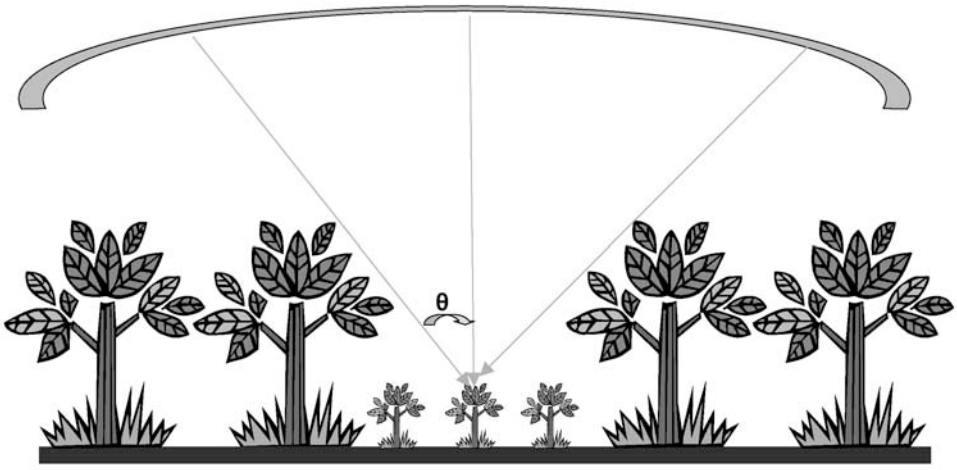

Figure 5. A schematic representation of transmission of direct diffuse radiation within gaps.

indirect diffuse radiation (R_{di}, the diffuse radiation transmitted through the surrounding forest) is given by:

$$\tau_{di} = 2\int_{\theta}^{\frac{\pi}{2}} G \cdot \sin\psi \cdot \cos\psi \cdot d\psi = 2G\int_{\sin\theta}^{\sin\frac{\pi}{2}} \sin\psi d\sin\psi$$
$$= 2 \cdot G\left(\frac{1}{2} - \frac{\sin^2\theta}{2}\right) = G\cos^2\theta \quad (19)$$

and then G is approximated by the averaged gap fraction of the surrounding forest, which is the gap fraction of the intact forest (i.e., gap_{intact}) in this case.

[39] The light-use efficiency of gap species varies with the changing fractions of R_{beam}, R_{dd}, and R_{di} in the total incoming radiation within the gap. Again, such a change in light-use efficiency is described by equation (16), with the fraction of diffuse radiation given by:

$$f_{\text{diff}} = \begin{cases} (R_{\text{dd}} + R_{\text{di}})/(R_{\text{beam}} + R_{\text{dd}} + R_{\text{di}}), & \text{for the sunlit understory} \\ 1, & \text{for the shaded understory} \end{cases} \quad (20)$$

[40] The radiative transfer module, combined with the regrowth module (described earlier), provides a 3-D representation of the forest canopy throughout the disturbance and recovery processes, allowing for a more detailed analysis of C storage and fluxes after selective logging.

3. Model Tests

3.1. Model Setup

[41] We tested CASA-3D on two experimental forest plots in the Tapajos National Forest, located south of Santarém in the state of Pará, Brazil. Mean annual precipitation is ~2000 mm, and mean annual mean temperature is ~25°C [*Silver et al.*, 2000]. One 97 ha plot served as a control, where no logging activity has occurred. Before logging, the mean gap fraction of the control and logged plots are 0.017 (σ = 0.04) and 0.018 (σ = 0.04), respectively, where σ represents the standard deviation. The second 98 ha plot was selectively logged in September 2000 [*Keller et al.*, 2004b] and its mean gap fraction became 0.24 (σ = 0.10) after the disturbance. Both of the plots are within 3 km from an eddy covariance tower, where precipitation, temperature, and solar radiation were monitored from July 2000 to February 2004 [*Miller et al.*, 2004; *Goulden et al.*, 2004; *da Rocha et al.*, 2004]. Using these meteorological measurements, we calculated a mean annual forcing time series of 12 months. CASA-3D was then initialized by repeatedly feeding the mean meteorological data into the model for 500 years, to generate a steady state for all C pools. The same forcing data were then used to drive a simulation of 40 years for a dynamic regrowth of the forest following selective logging. Landsat imagery for prelogging (10 August 1999) and postlogging (12 August 2000) triggered the forest disturbance in the model. We assumed that the climate over this region did not change significantly throughout the simulation. Although the model was run at a monthly time step, a monthly mean diurnal cycle for each month was embedded in the simulation as discussed earlier, so that the daily light environment could be simulated.

3.2. Comparison of Modeled and Measured C Stocks and Fluxes

[42] We compared our modeled estimates (spin-up simulations) of several C pools and fluxes to data available in the literature and/or from the Tapajos forest sites, which are listed in Table 1. In our model spin-up studies, we adjusted the parameters listed in Appendix A manually to best match simulated and measured NPP, C storage (NEP), and standing biomass-C stocks. A degree of uncertainty of high (H), medium (M), or low (L) was assigned to each parameter, which represents the uncertainty of the parameter from an ecological point of view. After this model calibration, our adjusted turnover times for leaf and wood were 2 and 52 years, respectively; the fractional allocation of NPP to the live carbon pools P_w, P_f, and P_r were 0.35, 0.30, 0.35, respectively; the turnover rates of the CWD pools were 0.21, 0.25, and 0.47 y^{-1} for large, medium, and small CWD pools, respectively.

[43] Table 1 displays the results of the spin-up and logging simulations. Since no logging occurs in the control or logged

Table 1. Carbon Budgets of the Simulations of the Control and Logged Plots at Tapajos

		Control Plot	Logged Plot							
	Values for Calibration	Spin-up/Simulation	Spin-up	1 year	2 years	5 years	10 years	20 years	30 years	40 years
Annual NPP (Mg C/ha/a)	6.7–16.8 [*Clark et al.*, 2001]	10.9	10.9	9.4	9.9	10.0	10.0	10.1	10.1	10.1
AGB (Mg C/ha)	151–203 [*Clark et al.*, 2001]	169.3	169.1	155.6	155.6	155.6	155.6	155.8	156.0	156.2
Total biomass (Mg C/ha)	186 [*Keller et al.*, 2001]	184.0	184.0	169.1	169.1	169.3	169.4	169.6	169.8	170.1
CWD (Mg C/ha)	25.4 (prelogging) 38.1 (1 year postlogging) [*Keller et al.*, 2004]	27.7	27.7	36.7	35.3	32.3	29.1	26.5	25.7	25.5
Soil C (Mg C/ha)	31.92 [*Silver et al.*, 2000; *Olander et al.*, 2005]	31.5	31.4	31.8	32.1	32.5	32.4	31.4	30.6	30.1
Annual respiration (Mg C/ha/a)	N/A	10.9	10.9	12.0	11.0	10.8	10.6	10.3	10.2	10.1
Annual NEP (Mg C/ha/a)	$-(0.8 \pm 2)$ [*Miller et al.*, 2004]	0.0	0.0	−2.6	−1.0	−0.8	−0.5	−0.2	−0.1	0.0

plot during model spin-up, their C budgets are essentially the same (Table 1). Slight differences between the plots result from natural variation in gap fractions in the remote sensing imagery of each site. In the control site the spin-up and main simulation runs were the same since there was no logging in either period.

[44] In the coarsest of our comparisons, data from *Clark et al.* [2001] provided a range of likely NPP values for Brazilian Amazon forests of 6.7–16.9 Mg C/ha/a, compared to 10.9 Mg C/ha/a from CASA-3D under undisturbed case. They also estimated aboveground biomass at 151–203 Mg C/ha, compared to 169.3 Mg C/ha and 169.1 Mg C/ha from the model for the control and logged plots, respectively. *Keller et al.* [2001] estimated biomass in and around our test sites within the Tapajos National Forest. Their estimates of total biomass were 186 Mg C/ha, and with a conservative error estimate of 50% uncertainty, while the estimate from the model is 184 Mg C/ha. In addition, *Keller et al.* [2004b] studied the volume and density of fallen CWD in undisturbed forest and logged forest 1 year after logging at Tapajos. CWD at Tapajos averaged 25.4 Mg C/ha and 38.1 Mg C/ha in undisturbed and logged forest (measured ~1 year postharvest), respectively, while CWD estimated from the model is 27.7 Mg C/ha under undisturbed circumstances and is 36.7 Mg C/ha at 1 year postharvest. *Miller et al.* [2004] estimated net C exchange in undisturbed forests at Tapajos, finding the forest to be a small source, or at most a modest sink, of carbon; their estimates of net ecosystem production (NEP) were -0.8 ± 2 Mg C/ha/a, where negative sign indicates C loss from the forest. *Saleska et al.* [2003] used eddy covariance methods to show that undisturbed forest in Tapajos was a small C source between July 2000 and August 2003. Finally, *Silver et al.* [2000] investigated effects of soil texture on belowground C and nutrient storage at Tapajos, showing that soil organic C in the top 30 cm averages 31.9 Mg C/ha prior to logging, while the soil C from the model is 31.5 Mg C/ha and 31.4 Mg C/ha at the control and logged plots, respectively. *Olander et al.* [2005] measured soil organic C pools within 1–2 years after logging at Tapajos and found no significant decrease in soil C stocks on that short timescale.

[45] Our initial results showed that logging has a significant effect on C pools and fluxes (Table 1). We use the sign convention where a positive indicates C sequestration, and a negative represents a net C loss from the system. In the 40-a simulation period after timber harvest, annual NPP recovered from 9.4 Mg C/ha/a in the first year following harvest to 10.1 Mg C/ha/a in the 40th year after logging. These values are well within the reported range provided by *Clark et al.* [2001]. Annual heterotrophic respiration had the largest values of 12.0 Mg C/ha/a in the first year after logging, and slowly decreased to 10.1 Mg C/ha/a by the 40th year. Annual NEP changed sign from a prelogging value of 0.0 Mg C/ha/a to −2.6 Mg C/ha/a in the first year after harvest, then it slowly approached a balanced 0.0 Mg C/ha/a by the 40th year. Our NEP results fell within the range measured by *Saleska et al.* [2003] and *Miller et al.* [2004]. In sum, our simulated changes in NPP, respiration, and NEP suggested that the logged forest site would be a net C source for 30 years following disturbance. Although the simulated forest is recovering after disturbance, the net rate of biomass accumulation is slow so that it would take at least four decades for the forest to reach a new quasi-steady state, which is roughly the value provided by *Silva et al.* [1995] for the same forested area at Tapajos. C pools were also altered after incorporating the remotely sensed canopy damage caused by selective logging (Table 1). The CWD pools rapidly increased from 26.7 to 36.7 Mg C/ha in the first year following harvest and then decreased to 25.5 Mg C/ha by the end of the 40th year. These values agree well with the field measurements provided by *Keller et al.* [2004b]. The soil C pools also showed a negligible change after logging, consistent with field measurements [*Olander et al.*, 2005].

[46] Table 1 only shows changes in the averaged C pools and fluxes at the site (~100 ha) scale. To evaluate the model's performance in simulating forest dynamics at the localized plot level, we selected three pixels with canopy gap fractions following logging of ~20%, 30%, and 60% within the logged plot. Figures 6a–6b illustrate the changes in gap fractions of the entire pixel and of the regrowth portion of the canopy only. Logging occurs in month 0, and gap fraction of the entire pixel suddenly increases, and then gradually recovers to its prelogging level in 1–1.5 years [*Asner et al.*, 2004]. Time series of gap fractions in each pixel were calculated based on equation (8) and shown in Figure 6a. The logged (damaged) fraction of each pixel is then inferred from equation (9) and the time series of the logged (or regrowing) portion of the pixel were calculated based on equation (10), which are shown in Figure 6b.

[47] These simulated changes in gap fraction corresponded to a suppression in NPP at the pixel level. Prior to logging, NPP in the three test pixels averaged 1.0 Mg C/ha/month, but pixels with a lower damage level (lower postlogging gap fraction) maintained higher NPP after

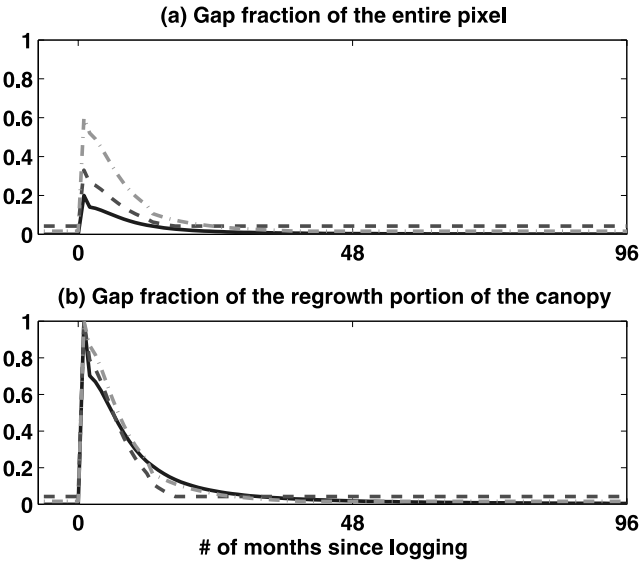

Figure 6. Change of (a) gap fraction of the entire pixel and (b) gap fraction of the regrowth portion of canopy before and in 96 months after logging at three selected pixels with logged fractions of 20% (solid line), 30% (dashed line), and 60% (dot-dashed line), respectively.

harvest (Figure 7a). Following logging, NPP in each pixel was calculated for the intact and logged portions separately and then summed to estimate total NPP. The NPP of the intact part was scaled by $1 - f_{\text{logged}}$ (Figure 7b), whereas NPP of the logged fraction was scaled by f_{logged} (Figure 7c).

[48] Figure 7 highlights our observations that NPP in pixels with higher damage levels returns to prelogging levels most rapidly because the larger canopy openings in those pixels allow more light to penetrate into the gaps for photosynthesis. As shown in Figures 7a and 7c, NPP increases at a higher rate at pixels with larger logged fractions. Interestingly, *Pereira et al.* [2002] and *Asner et al.* [2004a, 2004b] documented similar trends in terms of photosynthetic leaf area across hundreds of logged pixels. Similarly, *Asner et al.* [2006] remotely measured more rapid canopy closure in high-damage than in low-damage pixels throughout the Brazilian Amazon. However, our simulations also showed that following logging, pixel-scale NPP drops to a level proportional to $1 - f_{\text{logged}}$ so that a pixel with a higher logged fraction f_{logged} would have a lower NPP level. This modeling result is corroborated by time series field measurements of photosynthetic leaf area in low- to high-damage logging scenarios [*Pereira et al.*, 2002; *Asner et al.*, 2005a, 2005b].

[49] Results for heterotrophic respiration and NEP simulations in the three test pixels are shown in Figures 7d and 7e, respectively. The respiration in pixels with larger gap fractions was higher in the initial 2–3 years following logging due to the large pools of CWD and other surface C pools. However, at around 6th year after harvest, respiration rates from the three pixels became the same. By 10–15 years after harvest, respiration rates from pixels with larger gaps dropped to levels that were lower than pixels with smaller gaps. As a consequence of faster NPP recovery, higher initial respiration and lower respiration in later years, the pixels with larger gap fractions (higher damage levels) were initially a larger C source immediately following logging, but then recover to near neutral levels within a similar time frame as those pixels with smaller initial gap fractions (Figure 7e). The corresponding change in aboveground C stocks within each pixel is shown in Figure 8. After logging, aboveground C in all the logged pixels was reduced because a substantial fraction of the wood C pool was extracted and shipped to offsite sawmills, or it was damaged and entered the CWD pools. Those C fluxes were calculated based on equations (3)–(7). Changes in total aboveground C, and its fraction belonging to the intact portion of the forest in each pixel (weighted by $1 - f_{\text{logged}}$), as well as the logged portion (weighted by f_{logged}), are illustrated in Figures 8a, 8b, and 8c, respectively. With its faster rate of NPP recovery, aboveground C stocks in the pixel with 60% logged fraction also accumulated faster than the other two pixels with lower initial damage levels.

[50] In field studies, and thus in CASA-3D, three distinct plant functional types contribute to the regrowth dynamics of tropical forests following disturbance and logging: (1) pioneers, (2) shade-tolerant species, and (3) light-demanding species. The latter functional types include cohorts that may or may not reach upper-canopy positions in the forest. Figure 9 shows the CASA-3D aboveground biomass

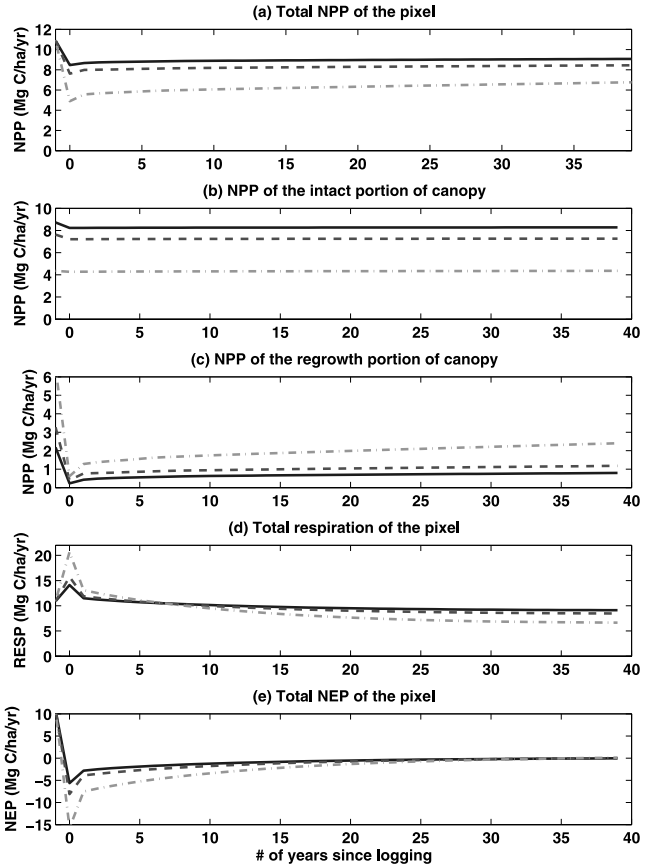

Figure 7. Change of (a) total NPP, (b) NPP of the intact portion of canopy, (c) NPP of the regrowth portion of canopy, (d) total respiration, and (e) total NEP before and after logging at three selected pixels with logged fractions of 20% (solid line), 30% (dashed line), and 60% (dot-dashed line), respectively.

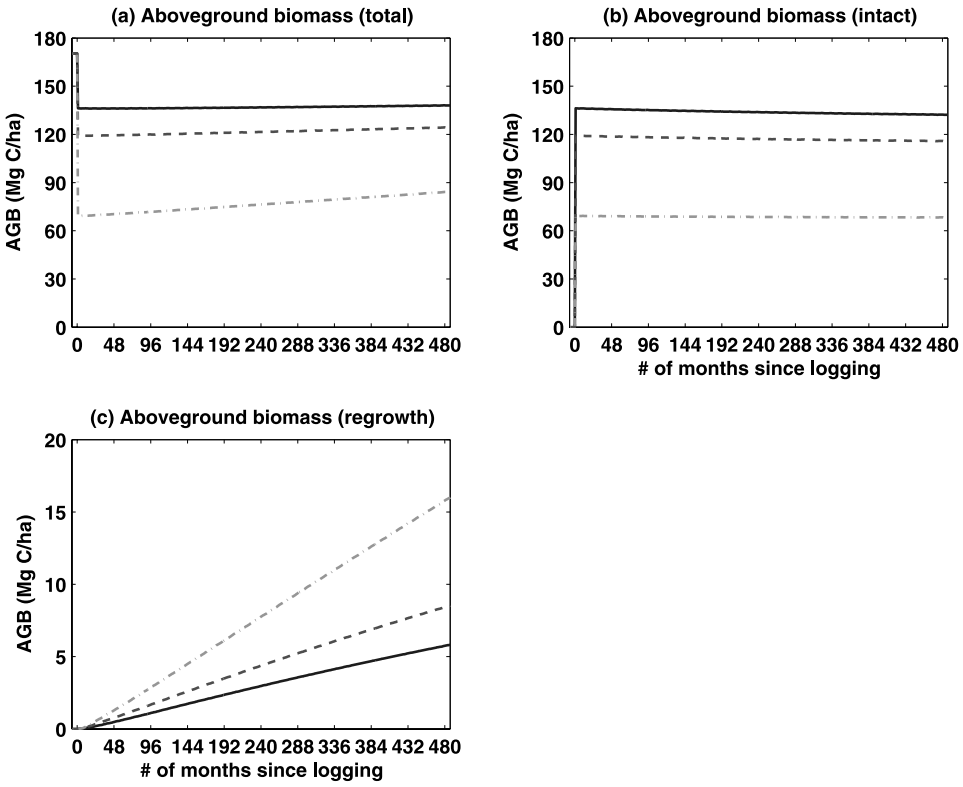

Figure 8. Change of (a) total AGB, (b) AGB of the intact portion of canopy, and (c). AGB of the regrowth portion of canopy at three selected pixels with logged fractions of 20% (solid line), 30% (dashed line), and 60% (dot-dashed line), respectively.

(AGB) simulations of these five groups following logging at 20%, 30%, and 60% of the pixel area. The AGB of pioneers accumulated rapidly in the first four years following disturbance and decreased thereafter (Figure 9a) because pioneers have high light-use efficiency but also high mortality rates. The AGB of both the shade-tolerant and light-demanding species steadily increased throughout the simulation period following logging (Figures 9b and 9c), whereas AGB of subcanopy trees initially increased but then leveled off as understory radiation levels decreased during the regrowth simulation (Figures 9d and 9e). However, the simulations also showed that subcanopy, shade-tolerant trees remained productive for much longer than did the light-demanding species. This result mirrors field-based observations of *Vieira et al.* [2005].

[51] Figure 10 illustrates the change of stem densities within the three selected pixels after logging. Pixels with greater logging intensity have higher overall stem densities in the resulting forest gaps because more light is able to pass through the larger openings. The stem densities of shade-tolerant and light-demanding species in all three pixels were identical as shown in Figures 10c and 10d. Thus for a pixel with a logged fraction <25%, the resulting initial stem density is the same as that of the pixel with a logged fraction of 20% (solid line). If the logged pixel fraction is >25%, pioneer species establish with a stem density proportional to the logged fraction within the pixel, as shown in Figure 2. In addition, Figures 10e and 10f demonstrate that if the logged fraction is very large, more trees establish and grow into the canopy. Intuitively, this result seems reasonable because higher light levels occur in larger gaps, which likely support higher levels of initial tree establishment.

4. Sensitivity Analyses and Uncertainties

[52] To understand the importance of various input factors associated with regrowth in CASA-3D, we first tested the absolute sensitivity of modeled NPP and respiration to a range of parameters. We then tested the relative sensitivity of the most important factors regulating NPP and respiration. Uncertainties in the simulated NPP and respiration were then estimated based on results from the sensitivity analyses.

4.1. Sensitivity Analyses

[53] We considered 13 factors (including model parameters and variables) in the sensitivity analyses (Table 2), and some of these factors were combined into groups during the analyses. For example, the maximum light-use efficiencies of the three functional types were grouped during the sensitivity analyses. That is, when $\varepsilon^*_{\text{pioneers}}$ was increased by 20% from its mean value, $\varepsilon^*_{\text{st}}$ and $\varepsilon^*_{\text{ld}}$ were also increased by 20%. Other factors, such as gap fraction, were treated individually. As shown in Table 2, 22 parameters were evaluated in the sensitivity analyses, and they were selected based on the degree of uncertainty in Appendix A.

[54] In the absolute sensitivity analyses, for each factor, 500 Monte Carlo simulations were executed by randomly varying the factor uniformly within its given range with other factors fixed (as shown in Table 2). Therefore in the

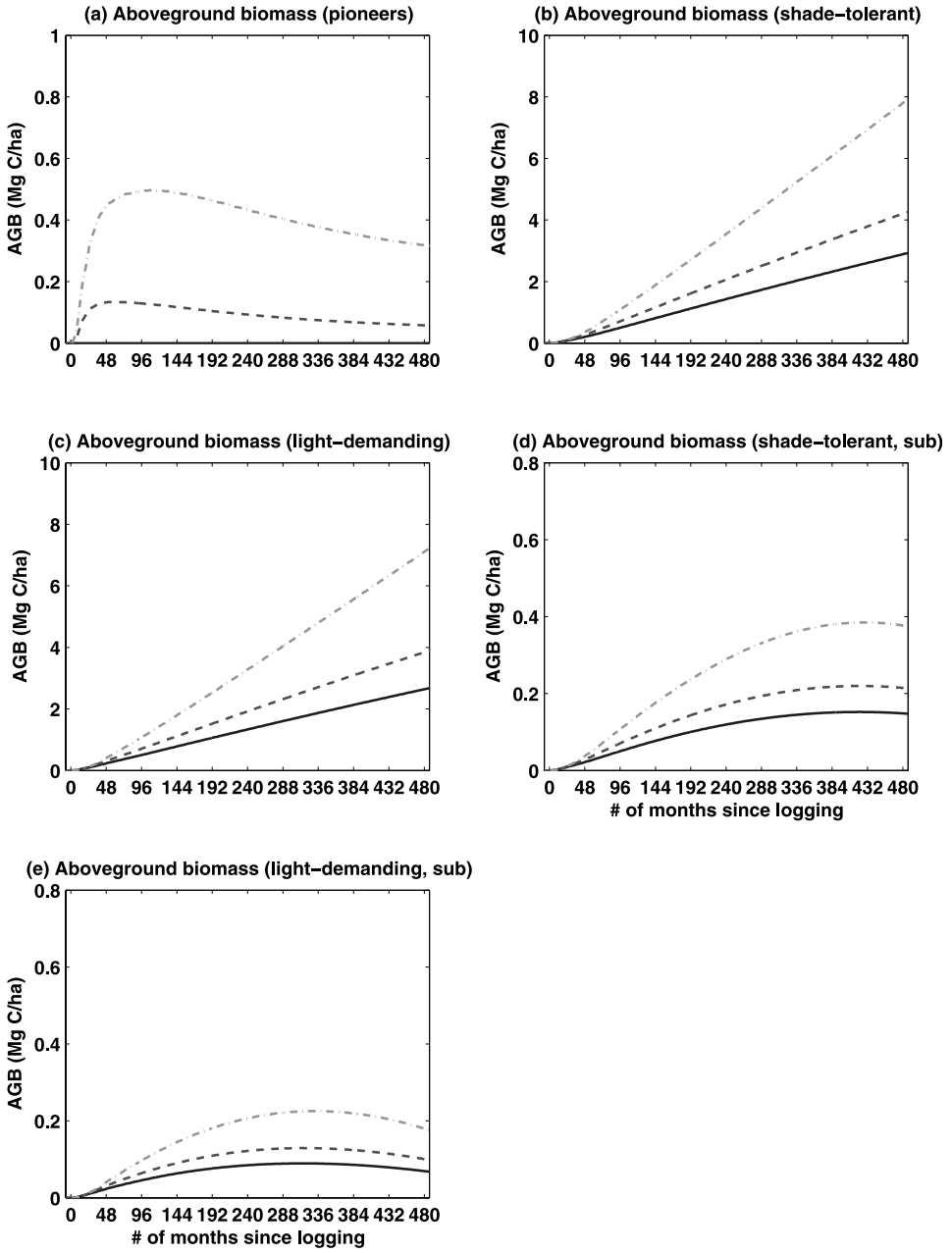

Figure 9. (a) AGB of the pioneer species; (b) AGB of the shade-tolerant species; (c) AGB of the light demanding species; (d) AGB of the subcanopy portion of the shade-tolerant species; (e) AGB of the subcanopy portion of the light demanding species in the regrowing forest at three selected pixels with logged fractions of 20% (solid line), 30% (dashed line), and 60% (dot-dashed line), respectively.

absolute sensitivity analyses, 500 × 13 simulations were executed. In the relative sensitivity analyses the contribution of each tested factor was evaluated by randomly selecting all the factors of interest within their respective ranges 500 times in order to obtain NPP and respiration for 500 base scenarios. For every base scenario, each group of factors in Table 2 was, in turn, perturbed by ±10% of its value, and the simulation repeated. The ±10% range was selected based on the notion that a smaller range in each variable would be difficult to detect in observation. A database was created for all model simulations with a total of 500 + 500 × 13 = 7000 simulations. Then the merit-of-change values (defined as the sum of the squares of differences) between the annual NPP or respiration from the base case scenarios and those from the perturbed simulations were recorded. A principle component analysis (PCA) was then performed on the 500 by 13 matrix with the merit-of-change values to reduce the dimension of such a matrix so that it is suitable for display in Figures 13 and 14. Since the first principal component axis represents the direction of maximum variance, the weighting of each perturbed factor's contribution to that axis was a measure of the model's sensitivity to the perturbed variable (see *Asner* [1998] and *Asner et al.* [2001] for details on the development and application of

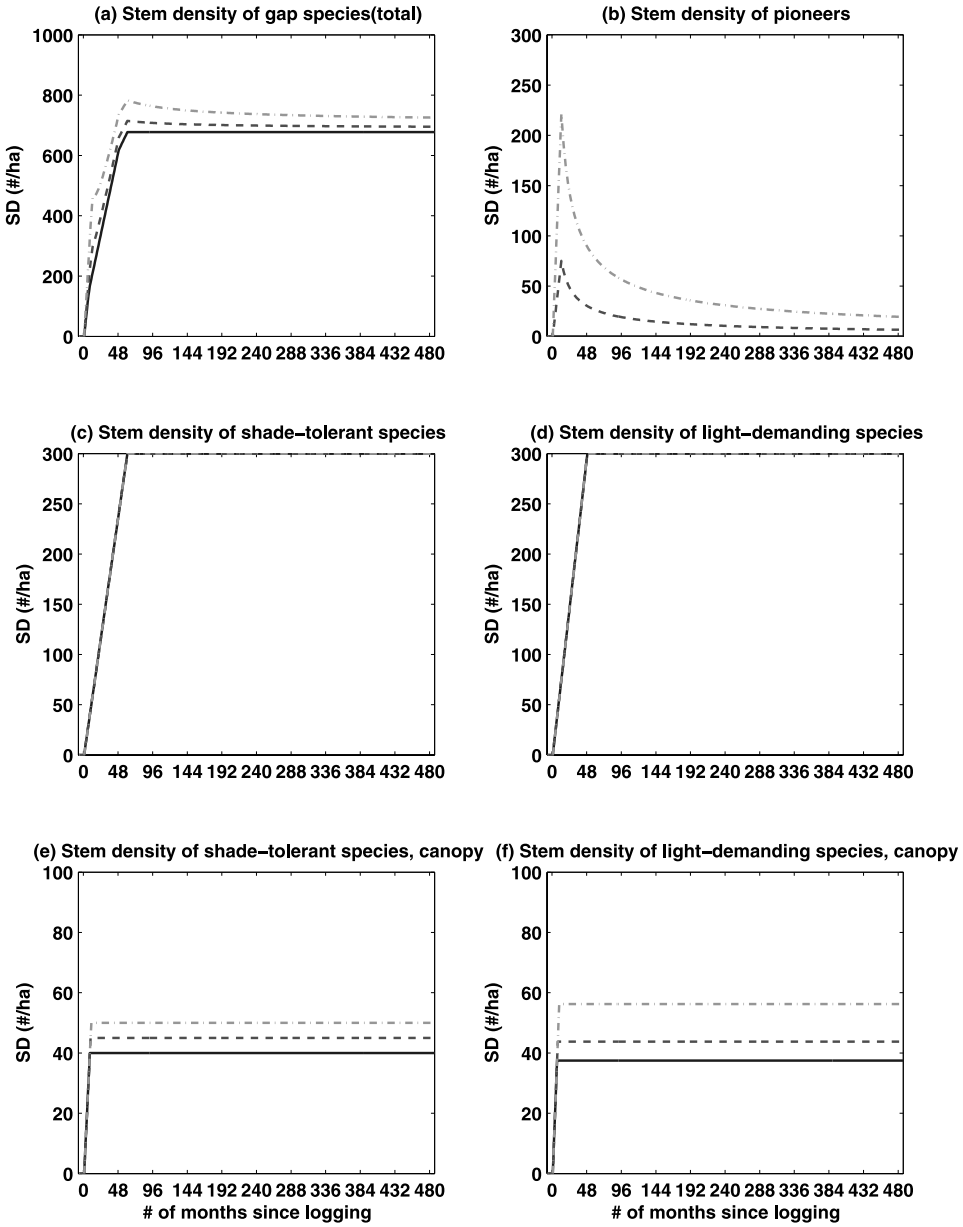

Figure 10. (a) Total stem density; (b) stem density of the pioneers; (c) stem density of the shade-tolerant species; (d) stem density of the light-demanding species; (e) stem density of the potential canopy trees of the shade-tolerant species; (f) stem density of the potential canopy trees of the light-demanding species after logging within three selected pixels with logged fractions of 20% (solid line), 30% (dashed line), and 60% (dot-dashed line), respectively.

this method). In both the absolute and relative sensitivity analyses, the sensitivity of 13 factors was assessed with respect to annual NPP and respiration at 1, 2, 5, 10, 20, 30, and 40 years after selective logging.

[55] The absolute sensitivity of NPP and respiration are shown in Figures 11 and 12, respectively. From Figure 11, it is clear that gap fraction is the most important factor controlling NPP in disturbed forest. The maximum light-use efficiencies of the gap species, the meteorological variables, and the GOMS parameters played a secondary role in determining NPP for years following timber harvest. The impact of other regrowth parameters (i.e., rho, SD, T_p, allocation of NPP, and gap_{th}) was small. Canopy gap fraction affects NPP in our model because it controls (1) the absorbed photosynthetically active radiation, (2) the species composition in gaps, and (3) the light transmission into gaps as simulated with the radiative transfer module. Gap fraction was also the most important factor determining heterotrophic respiration after logging. The decay rates of coarse woody debris and the allocation of NPP into leaf, wood, and root carbon pools also contributed significantly to respiration in the initial stage of regrowth, but their importance decreased after 10 years of regrowth. The impact of the regrowth parameters (i.e., LUE, rho, SD, T_p) and the GOMS parameters was increasing with the regrowth in the logged portion. Gap fraction affects respiration in the model

Table 2. List of Factors for Sensitivity Analyses

Factors	Meaning	Parameters Included	Mean Value ± Error
LUE	Maximum light-use efficiency	$\varepsilon^*_{pioneers}$	0.50 gC MJ^{-1} ± 20%
		ε^*_{st}	0.42 gC MJ^{-1} ± 20%
		ε^*_{ld}	0.38 gC MJ^{-1} ± 20%
rho	Specific density of wood	$\rho_{pioneer}$	0.4 g cm^{-3} ± 20%
		ρ_{st}	0.6 g cm^{-3} ± 20%
		ρ_{ld}	0.45 g cm^{-3} ± 20%
SD	Maximum stem density of primary species	$SD1_{st}$	300 ± 50 stems/ha
		$SD1_{ld}$	300 ± 50 stems/ha
Tp	Time for primary species to reach SD	T_{p_st}	5 ± 1 years
		T_{p_ld}	4 ± 1 years
age_pioneers	Average age of woody tissues of pioneers	$Pioneer_{age}$	10 ± 4 years
ppt	Precipitation	–	Mean monthly value ± 20%
airt	Air temperature	–	Mean monthly value ± 10%
solrad	Solar radiation	–	Mean monthly value ± 10%
gap	gap fraction	gap_0	0–0.8
allocation	Allocation of NPP to live carbon pools	P_f	0.30 ± 0.025
		P_r	0.30 ± 0.025
		P_w	$1 - P_f - P_r$
k_cwd	Decay rates of the CWD pools	k_{cwd_large}	0.21 yr ± 10%
		k_{cwd_medium}	0.25 yr ± 10%
		k_{cwd_small}	0.47 yr ± 10%
gap_{th}	Threshold of gap fraction agove which pioneer species can be found	gap_{th}	0.25 ± 0.1
goms	Parameters in the GOMS module	b	8.74 ± 0.5
		h	26.38 ± 1.0
		brratio	0.63 ± 0.06

because: (1) the damaged fractions of wood, leaf, and root carbon pools caused by logging are linked to the postlogging gap fraction of each pixel; and (2) the larger gaps with more pioneer species turnover quickly and serve as a source of C back to the atmosphere.

[56] The results from the relative sensitivity analysis are shown in Figures 13 and 14. Only the factors with PCA weights larger than 10^{-4} are shown. Gap fraction and the GOMS parameters had the largest impact on simulated NPP after logging. The control of gap fraction on NPP became less and less important after the initial recovery in foliage and establishment of species in the gaps. Similarly, the impact of gap_{th} was significantly in the first year through its control over species composition. The GOMS parameters started to take over after 10 years because they regulated the light transmission into the regrowth forest. The parameters controlling the regrowth of the gap species (i.e., LUE, rho, allocation of NPP, SD, T_p) and the meteorological variables (i.e., airt, ppt, solrad) on NPP also had measurable impacts on NPP. The regrowth parameters became more and more important after 10 years of regrowth.

[57] Gap fraction and the GOMS parameters also played a major role in controlling respiration, but the CWD decay rates were dominant factors in the initial five years after logging. Air temperature and the allocation of NPP became significant factors by the 10th year following simulated timber harvest. The maximum light-use efficiencies also affected respiration, especially by the 20th year following disturbance. The other regrowth parameters and meteorological variables contributed to the respiration too, although with much smaller weights. Gap fraction determined the amount of C in the detrital C pools available for respiration in a relative short period (i.e., 10 years) after the disturbance, and the GOMS parameters and the regrowth parameters affected respiration through their control on NPP and eventually on carbon that is available for turnover and respiration in late stages of regrowth.

[58] The relative and absolute sensitivity analyses point to the same factors. The maximum sensitivity of model productivity to forest canopy gap fraction was most pronounced in the relative sensitivity simulations; even when there is only a 10% bias in gap fraction from satellite imaging, the simulated carbon budget is significantly altered. Simulated NPP and respiration in late stages of regrowth were also very sensitive to the GOMS parameters, which interacted with the canopy gap fraction closely through λ. Therefore it is critical for us to control the quality of gap fractions obtained from the CLAS remote sensing approach because a small error in gap fraction would propagate and introduce large uncertainty to the simulated carbon pools and fluxes.

4.2. Uncertainties

[59] Table 3 summarizes the uncertainties in simulated annual NPP and respiration associated with the 13 factors in the absolute sensitivity analysis. To estimate the uncertainties, the mean and standard deviation of annual NPP and respiration from the 500 Monte Carlo simulations for each factor were calculated and the error corresponding to the 95% confidence interval was estimated as:

$$E_a = 100 \times (1.96 \times \sigma/\bar{x}) \tag{21}$$

where $\bar{x}$ and σ are the mean and standard deviation of annual NPP or respiration.

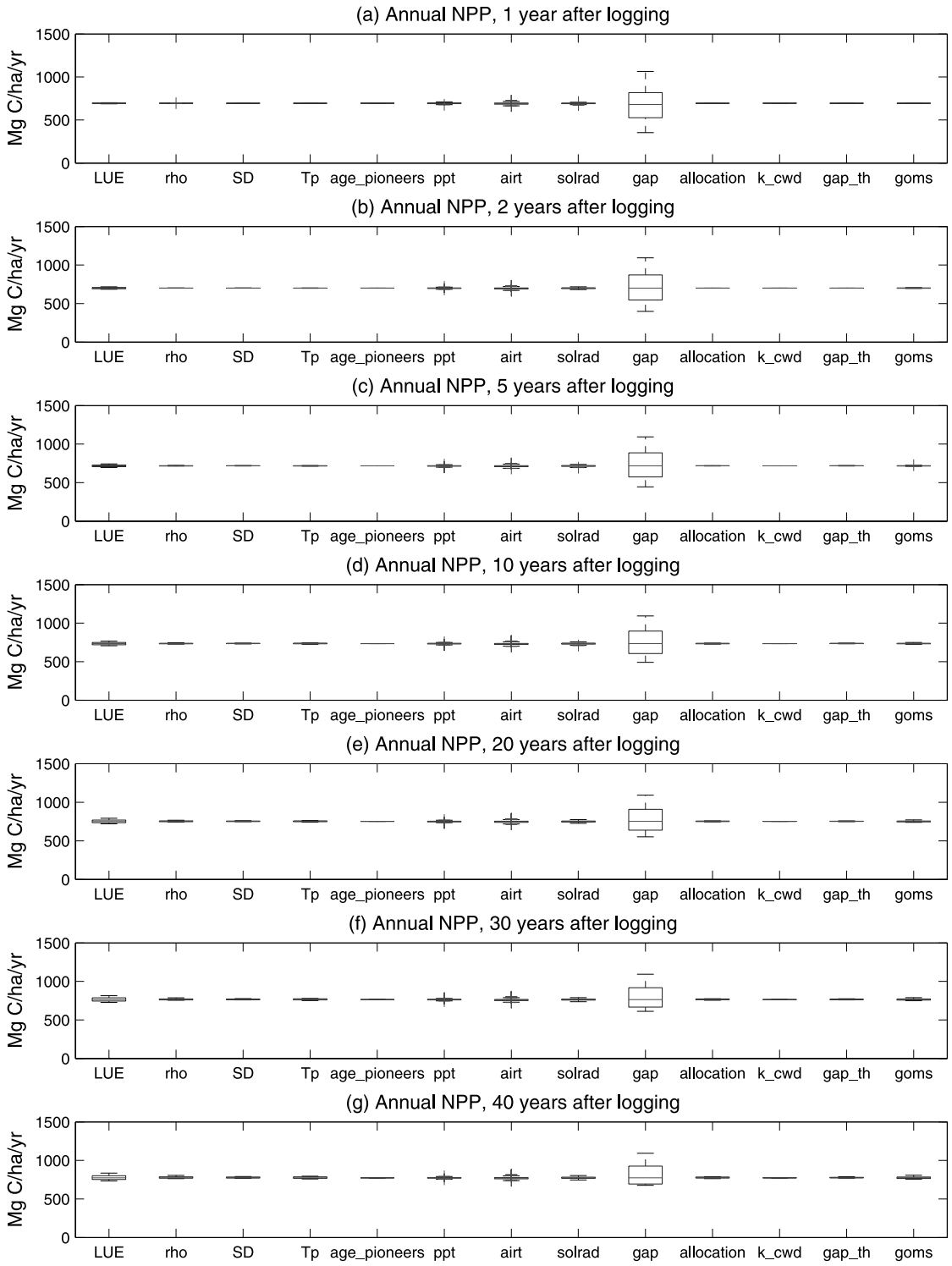

Figure 11. Absolute sensitivity of annual NPP to different factors in (a) 1 year, (b) 2 years, (c) 5 years, (d) 10 years, (e) 20 years, (f) 30 years, and (g) 40 years after logging.

[60] With the mean parameter values and error estimates of the 13 factors given in Table 2, the uncertainties of simulated NPP and respiration associated with each factor were different. Gap fraction introduced the largest uncertainty to the simulated NPP and respiration. The error can be as large as 58.2% for NPP and 52.3% for respiration with gap fraction varying between 0 and 0.8. The CWD decay rates affected respiration by 6–9% in the first 5 years after timber harvest and its impact decreased thereafter. The uncertainty introduced by the meteorological variables was about 3% for NPP and 2% for respiration. The impacts of all regrowth parameters (i.e., LUE, rho, T_p, SD, alloca-

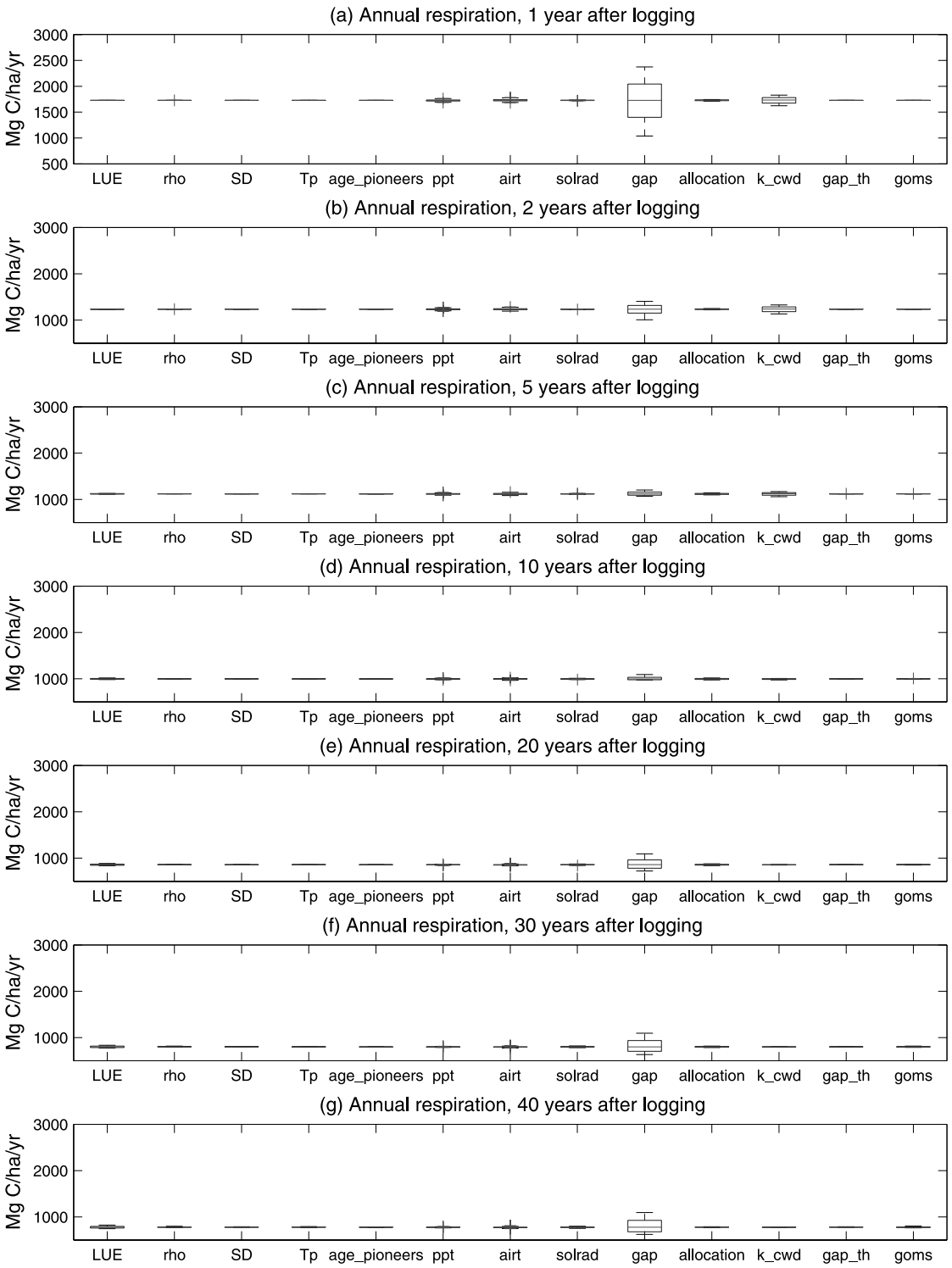

Figure 12. Absolute sensitivity of annual respiration to different factors in (a) 1 year, (b) 2 years, (c) 5 years, (d) 10 years, (e) 20 years, (f) 30 years, and (g) 40 years after logging.

tion of NPP, gap_{th}) and the GOMS parameters were increasing with the regrowth of the forest. The maximum light use efficiencies introduced up to 7% and 5% uncertainty to NPP and respiration, respectively. The specific densities of timbers and T_p affect NPP by up to 3% and respiration by up to 2%. The GOMS parameters could introduce up to 3% uncertainty to NPP and 2% to respiration. Other parameters (i.e., SD, allocation of NPP, gap_{th}) had smaller effect on simulated NPP and respiration.

[61] The uncertainties associated with the 13 factors in the relative sensitivity analysis were estimated with the following procedure:

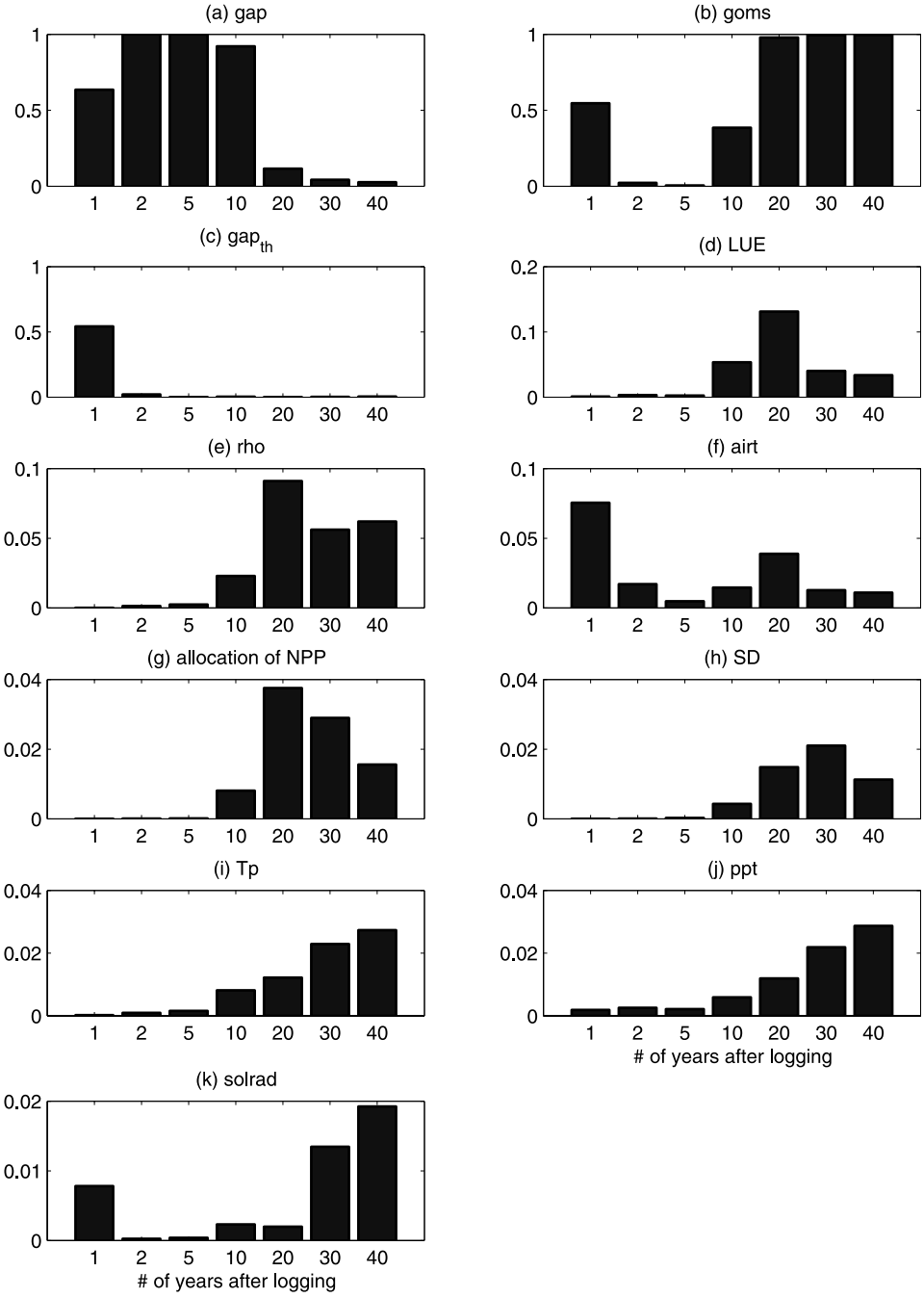

Figure 13. Relative sensitivity of NPP to (a) gap fraction, (b) goms, (c) gap_{th}, (d) LUE, (e) rho, (f) air temperature, (g) allocation of NPP, (h) SD, (i) T_p, (j) precipitation, and (k) solar radiation in different years after logging. Note that the scales of y axes vary among the figures for a clear presentation.

[62] (1) Calculate the error associated with each of the 13 factor as:

$$x'_j = \left(x_j - x_j^b\right)/x_j^b \tag{22}$$

where $j \in (1, \cdots, 500)$ is the index of the Monte Carlo simulations for the factor of interest, x_j^b is the simulated NPP or respiration from the jth base scenario, and $x_{i,j}$ is that from jth simulation;

[63] (2) Calculate the standard deviation σ of x'_j;

[64] (3) The uncertainty corresponding to the 95% confidence interval is then given by:

$$E_r = 100 \times (1.96 \times \sigma) \tag{23}$$

[65] The values of E_r are listed in Table 4 and represent the uncertainties associated with the 13 factors when each factor was perturbed by ±10% within its range. Gap fraction introduced up to 15% and 7% uncertainty for NPP and respiration, respectively, by the first year after timber harvest. The impacts of the GOMS parameters were relative

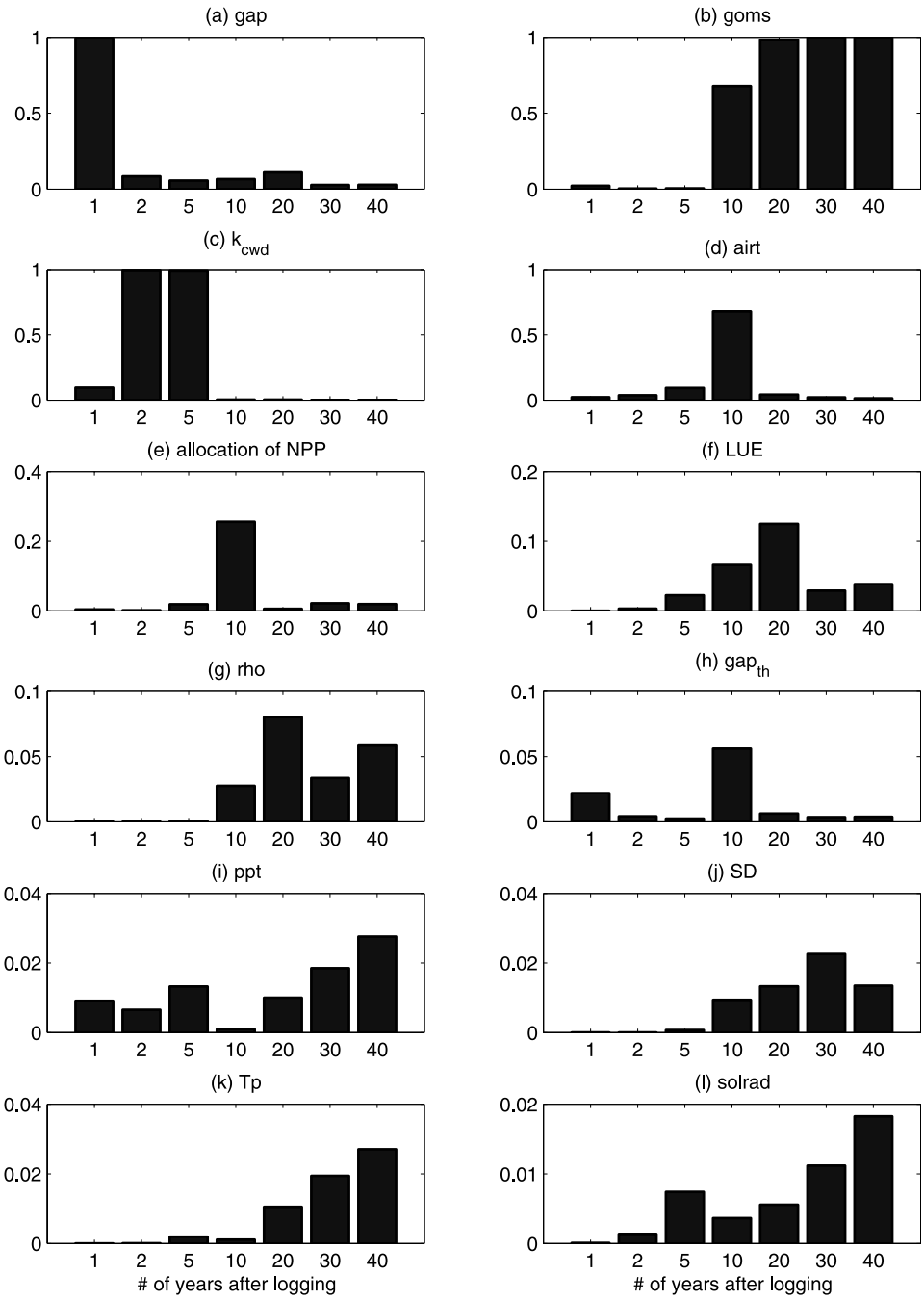

Figure 14. Relative sensitivity of respiration to (a) gap fraction, (b) goms, (c) k_{cwd}, (d) air temperature, (e) allocation of NPP, (f) LUE, (g) rho, (h) gap_{th}, (i) precipitation, (j) SD, (k) T_p, and (l) solar radiation in different years after logging. Note that the scales of y axes vary among the figures for a clear presentation.

small in the first few decades but gradually increased to 19% for NPP and 14% for respiration by the 40th year of regrowth. gap_{th} affected NPP significantly by 9% by the first year after timber harvest. The uncertainty introduced by maximum light use efficiencies increased from 1% and 0% by the first year after harvest to 8% and 6% by the 40th year for NPP and respiration, respectively. Solar radiation affected NPP by about 5% and respiration by about 4%, and its impact was the largest among the meteorological variables. Specific wood density and allocation of NPP could affect NPP by 5% and respiration by 4%. T_p and stem densities affected NPP by 4% and 3%, and respiration by 3% and 2%, respectively. Again, all regrowth parameters showed increasing impacts on simulated NPP and respiration with the regrowth, except for the age of pioneers, which seemed to have no impact on NPP or respiration.

5. Discussion

[66] CASA-3D was designed to simulate the effects of disturbance on carbon pools and fluxes in terrestrial ecosystems, and to do so at high spatial resolution commensu-

Table 3. Uncertainties Associated With the 13 Factors in the Absolute Sensitivity Analyses (E_a)

Factors		1 year	2 years	5 years	10 years	20 years	30 years	40 years
LUE	NPP	1.1	2.5	3.5	4.5	5.2	6.1	7.0
	RESP	0.0	0.3	1.0	2.0	3.1	4.2	5.2
rho	NPP	0.0	0.1	0.8	1.4	1.7	2.4	3.1
	RESP	0.0	0.0	0.2	0.6	0.9	1.5	2.2
SD	NPP	0.1	0.2	0.4	0.7	0.9	1.2	1.5
	RESP	0.0	0.0	0.1	0.3	0.5	0.8	1.1
T_p	NPP	0.1	0.3	0.6	1.3	1.5	2.1	2.8
	RESP	0.0	0.0	0.1	0.5	0.9	1.4	1.9
$age_{pioneer}$	NPP	0.0	0.0	0.0	0.0	0.0	0.0	0.0
	RESP	0.0	0.0	0.0	0.0	0.0	0.0	0.0
ppt	NPP	1.8	1.6	1.6	1.7	1.7	1.7	1.7
	RESP	1.5	2.1	1.8	1.4	1.0	1.0	1.2
airt	NPP	2.9	2.9	2.9	3.0	3.0	3.1	3.1
	RESP	2.0	2.5	2.2	2.0	1.9	2.1	2.4
solrad	NPP	1.6	1.9	2.1	2.3	2.3	2.5	2.7
	RESP	0.3	0.4	0.7	1.1	1.5	1.8	2.1
gap	NPP	52.3	58.2	54.7	49.9	44.6	40.0	35.8
	RESP	47.6	.17.8	.6.7	7.9	26.9	36.1	38.6
Allocation of NPP	NPP	0.0	0.1	0.5	0.9	1.0	1.5	1.9
	RESP	1.0	1.2	2.1	2.4	2.6	2.1	1.5
k_{cwd}	NPP	0.0	0.0	0.0	0.0	0.0	0.0	0.0
	RESP	6.8	9.0	5.5	1.9	0.8	1.0	0.7
gap_{th}	NPP	0.1	0.1	0.3	0.5	0.6	0.8	1.1
	RESP	0.0	0.0	0.0	0.2	0.3	0.5	0.7
goms	NPP	0.3	0.6	0.9	1.4	1.8	2.4	2.9
	RESP	0.0	0.1	0.2	0.6	1.0	1.5	2.0

rate with regional ecological studies incorporating high spatial resolution remotely sensed data. Compared to the original version of CASA, this new model includes: (1) an alternative approach for calculating APAR that takes advantage of the remotely sensed gap fraction at a spatial resolution of 28.5 m by 28.5 m; (2) a pulse-disturbance module to modify the carbon pools after a forest disturbance such as selective logging; (3) a module to simulate the regrowth of gap species considering community ecology; and (4) a crown radiative transfer module to simulate the dynamic light environment in the postdisturbance gaps.

[67] The regrowth module features a new set of parameterizations on the basis of field studies of gap dynamics in tropical rainforests [*Whitemore*, 1998; *Brokaw*, 1985, 1987], which have existed in literature for a few decades but not yet been implemented in any other ecosystem models. With these parameterizations, the simulation of gap phase regeneration at a landscape scale becomes possible without detailed site- and/or species-specific information. Gap phase regeneration is not only important under a human disturbance scenario but also in intact forests, which have been described as shifting mosaics of different-sized patches cycling through gap, building, and mature phases [*Brokaw*, 1985]. CASA-3D provide a means to simulate dynamic changes in forest architecture, composition, and tree population dynamics, all of which have profound effects on forest carbon cycles.

[68] We recognize that CASA-3D was developed with a number of assumptions and with the use of several simplified phenomenological relationships pertaining to community ecology of species and plant functional types. However, *Swaine and Whitmore* [1988] pointed out that when the species in a tropical forest ecosystem are grouped into a few coarse functional types, the characteristics or assumptions for these functional types can be made sufficiently general to facilitate their use and application in many tropical forest types. In this paper, species in tropical forest are categorized into three functional types, whose regrowth parameters can be adjusted based on field observations or through an inverse modeling approach. The relationship between gap size and community composition was documented in general terms by *Whitemore* [1998] for lowland rainforest as well as by *Brokaw* [1985, 1987] for Panamanian rainforests. Unfortunately, a detailed study of community composition in gaps, such as the one in the work of *Brokaw* [1985, 1987] is not available for the Brazilian Amazon. Therefore parameter values from Panama are our best knowledge available for species composition in tropical rainforest.

[69] Furthermore, from our results of sensitivity analysis in section 4, the model is not very sensitive to the parameters for community composition (i.e., SD, Tp, age of pioneers, etc.). Instead, gap fraction and the crown dimension (GOMS) parameters, which can be measured from remote sensing, had the most significant impact on model simulations. Therefore we felt it appropriate to apply the Panama parameterization to the Amazon sites, especially given that the emphasis of the model is on the carbon budget and not on species composition within postdisturbance gaps.

[70] With the new features in CASA-3D, now we are able to consider how different biophysical and physiological characteristics modulate the C cycle in pre disturbance and postdisturbance scenarios. In addition, by closely coupling an integrated set of parameterizations with remotely sensed canopy gap fraction from space, CASA-3D is suitable for applications at large scale such as the carbon cycle modeling of the entire Amazon Basin. We note that edge effects caused by gaps and impact of gaps on envi-

Table 4. Uncertainties Associated With the 13 Factors in the Relative Sensitivity Analyses (E_r)

Factors		1 year	2 years	5 years	10 years	20 years	30 years	40 years
LUE	NPP	1.4	2.5	3.6	4.2	5.8	7.0	8.4
	RESP	0.0	0.2	0.7	1.5	3.1	4.6	6.3
rho	NPP	0.0	0.2	1.0	1.4	3.0	3.9	5.1
	RESP	0.0	0.0	0.2	0.5	1.5	2.3	3.7
SD	NPP	0.1	0.2	0.5	0.6	1.2	1.9	2.6
	RESP	0.0	0.0	0.1	0.2	0.6	1.2	1.9
T_p	NPP	0.1	0.2	0.6	0.9	1.8	2.8	3.8
	RESP	0.0	0.0	0.1	0.3	0.9	1.8	2.7
$age_{pioneer}$	NPP	0.0	0.0	0.0	0.0	0.0	0.0	0.0
	RESP	0.0	0.0	0.0	0.0	0.0	0.0	0.0
ppt	NPP	0.9	0.9	1.0	1.0	1.3	1.7	2.0
	RESP	0.8	1.1	1.0	0.8	0.7	1.1	1.5
airt	NPP	3.0	3.1	3.2	3.3	3.5	3.8	4.1
	RESP	1.9	2.5	2.3	2.1	2.1	2.6	3.1
solrad	NPP	2.0	2.3	2.5	2.7	3.2	3.9	4.5
	RESP	0.4	0.5	0.8	1.2	1.8	2.7	3.5
gap	NPP	15.0	8.1	7.1	6.2	5.4	4.6	4.5
	RESP	6.8	3.0	1.1	1.1	3.2	4.0	4.4
Allocation of NPP	NPP	0.0	0.2	0.9	1.3	2.5	3.8	5.1
	RESP	0.8	1.1	1.8	2.0	2.0	2.2	2.8
k_{cwd}	NPP	0.0	0.0	0.0	0.0	0.0	0.0	0.0
	RESP	3.3	4.3	2.6	0.9	0.8	0.8	0.5
gap_{th}	NPP	9.1	0.6	0.3	0.3	0.5	0.8	1.1
	RESP	1.2	0.4	0.3	0.2	0.3	0.5	0.8
goms	NPP	9.2	1.9	4.1	6.9	12.0	15.7	19.2
	RESP	1.2	0.4	0.8	2.2	6.1	10.1	14.2

Table A1. Summary of Model Parameters, Their Values, and Ranges As Employed in CASA-3D

Parameter	Location in the Text	Degree of Uncertainty	Meaning and Citation	Mean ± Uncertainty (If Any)
			Parameters for Intact Forest	
litcn	–	L	Litter C/N ratio	24.5
lignin	–	L	Lignin fraction of litter	0.072
lrage	–	L	Average age of leaves and fine roots [*Hirsch et al.*, 2004]	2 ± 0.5, year
woodage	–	M	Average age of woody tissues [*Hirsch et al.*, 2004]	52 ± 5, year
laimax	–	L	Maximum LAI [*Nepstad et al.*, 2004]	5.7
P_w	–	H	Fraction of NPP allocated to wood [*Hirsch et al.*, 2004]	0.35 ± 0.04
P_f	–	H	Fraction of NPP allocated to foliage [*Hirsch et al.*, 2004]	0.30 ± 0.025
P_r	–	H	Fraction of NPP allocated to fine roots [*Hirsch et al.*, 2004]	0.35 ± 0.035
$k_{surfmet}$	–	L	Turnover rate of the surface metabolic pool [*Potter et al.*, 1993a, 1993b]	14.8 a^{-1}
$k_{surfstr}$	–	L	Turnover rate of the surface structure pool [*Potter et al.*, 1993a, 1993b]	3.9 a^{-1}
$k_{soilmet}$	–	L	Turnover rate of the soil metabolic pool [*Potter et al.*, 1993a, 1993b]	18.5 a^{-1}
$k_{soilstr}$	–	L	Turnover rate of the soil structure pool [*Potter et al.*, 1993a, 1993b]	4.9 a^{-1}
k_{cwd_large}	–	H	Turnover rate of the large CWD pool [*Palace et al.*, 2007]	0.21 a^{-1} ± 10%
k_{cwd_medium}	–	H	Turnover rate of the medium CWD pool [*Palace et al.*, 2007]	0.25 a^{-1} ± 10%
k_{cwd_small}	–	H	Turnover rate of the small CWD pool [*Palace et al.*, 2007]	0.47 a^{-1} ± 10%
$k_{surfmic}$	–	L	Turnover rate of the surface microbial pool	6.0 a^{-1}
$k_{soilmic}$	–	L	Turnover rate of the soil microbial pool	7.3 a^{-1}
k_{slow}	–	L	Turnover rate of the slow carbon pool [*Potter et al.*, 1993a, 1993b]	0.22 a^{-1}
$k_{passive}$	–	L	Turnover rate of the passive carbon pool [*Potter et al.*, 1993a, 1993b]	0.0045 a^{-1}
ε	equation (1)	M	Average light use efficiency of the intact forest [*Field et al.*, 1995]	0.40 gC/MJ ± 20%
			Parameters for Simulating Regrowth Within Gaps	
α_0	equation (8)	L	Parameter in the gap recovery function [*Asner et al.*, 2006]	*f*(*gap*)
α_1	equation (8)	L	Parameter in the gap recovery function [*Asner et al.*, 2006]	*f*(*gap*)
α_2	equation (8)	L	Parameter in the gap recovery function [*Asner et al.*, 2006]	*f*(*gap*)
$\varepsilon^*_{pioneer}$	–	H	Maximum light use efficiency of the pioneer species [*Field et al.*, 1995]	0.50 gC MJ^{-1} ± 20%
ε^*_{st}	–	H	Maximum light use efficiency of the shade-tolerant primary species [*Field et al.*, 1995]	0.42 gC MJ^{-1} ± 20%
ε^*_{ld}	–	H	Maximum light use efficiency of the light-demanding primary species [*Field et al.*, 1995]	0.38 gC MJ^{-1} ± 20%
$\rho_{pioneer}$	–	H	Specific wood density of the pioneer species [*Lawton*, 1984]	0.4 g cm^{-3} ± 20%
ρ_{st}	–	H	Specific wood density of the shade-tolerant primary species [*Lawton*, 1984]	0.6 g cm^{-3} ± 20%
ρ_{ld}	–	H	Specific wood density of the light demanding primary species [*Lawton*, 1984]	0.45 g cm^{-3} ± 20%
gap_{th}	equation (11)	M	The threshold of gap fraction above which pioneer species can be found [*Brokaw*, 1985]	0.25 ± 0.1
ISD_{max}	equation (11)	M	Maximum initial stem density of pioneer species one year after logging [*Brokaw*, 1985, 1987]	300 ± 50 stems/ha
ISD_{min}	equation (11)	M	Minimum initial stem density of pioneer species one year after logging [*Brokaw*, 1985, 1987]	50 stems/ha

Table A1. (continued)

Parameter	Location in the Text	Degree of Uncertainty	Meaning and Citation	Mean ± Uncertainty (If Any)
SD_{1_st}	section 2.3.1	H	Final stem density of shade tolerant primary species [*Silva et al.*, 1995]	300 ± 50 stems/ha
SD_{1_ld}	section 2.3.1	H	Final stem density of light demanding primary species [*Silva et al.*, 1995]	300 ± 50 stems/ha
SD_{0_st}	section 2.3.1	L	Initial stem density of shade tolerant primary species after logging	0 stems/ha
SD_{0_ld}	section 2.3.1	L	Initial stem density of light demanding primary species after logging	0 stems/ha
T_{p_ld}	section 2.3.1	H	Number of years for light-demanding species to reach the final stem density [*Brokaw*, 1985, 1987]	4 ± 1 year
T_{p_st}	section 2.3.1	H	Number of years for shade-tolerant species to reach the final stem density [*Brokaw*, 1985, 1987]	5 ± 1 year
$Pioneer_{age}$	section 2.3.1	H	Average age of woody tissues of pioneer species	10 ± 4 year
$ST\_understory_{age}$	section 2.3.1	L	Average age of woody issues of shade-tolerant species presented in the understory [*Vieira et al.*, 2005]	100 ± 20 year
$LD\_understory_{age}$	section 2.3.1	L	Average age of woody issues of light-demanding species presented in the understory [*Vieira et al.*, 2005]	25 ± 10 year
$f_{understory}$	section 2.3.1	M	Contribution in percentage of the understory trees to the total LAI of the primary species	10 ± 5%
$T_{understory}$	section 2.3.1	M	Number of years for the contribution of understory trees to the total LAI decrease from $f_{understory}$ % to 0%	40 ± 10 year
a_0, a_1, a_2, a_3	equation (12)	M	Parameters to estimate AGB of a tree of the primary functional types based on its DBH [*Chave et al.*, 2005]	−1.50, 2.48, 0.21, −0.03
c_1, c_2, c_3	equation (13)	M	Parameters to relate DBH with H (M. Keller, unpublished manuscript, year?)	3.63, 0.51, 1.17
a_4, a_5	equation (14)	M	Parameters to estimate AGB of the pioneer functional type based on its DBH [*Nelson et al.*, 1999]	−2.51, 2.43
Δ_{diff}	equation (16)	L	Parameter to modify ε based on light condition [*Anderson et al.*, 2000]	0.4 for C3 plants 0.15 for C4 plants
			Parameters for GOMS [*Asner et al.*, 2002b]	
r	section 2.4.2	H	Average crown radius	13.96/2 ± 0.4 m
b	section 2.4.2	H	Vertical half axis of the tree crown	8.74/2 ± 0.5 m
h	section 2.4.2	H	Height of canopy from ground to crown center of the intact forest	26.38 ± 1.0 m
h_{diff}	section 2.4.2	L	Height difference between intact trees and regrowing trees	$h - h_{rg}$
brratio	section 2.4.2	H	Crown vertical-to-horizontal diameter ratio	8.74/13.96 ± 0.06
hbratio	section 2.4.2	L	Crown height-to-vertical diameter ratio	h_{diff}/b
λ	section 2.4.2	L	Density of crowns per pixel	$(1 - gap(0))/(\pi r^2)$

ronment (e.g., temperature, soil moisture, etc.) were not considered in the current version of CASA-3D. We will investigate these factors in the future development of the model.

[71] Detailed studies at the pixel level show that regrowth following timber harvest is tightly regulated by the light environment in the postlogging gaps. Our sensitivity analyses showed that gap fraction, the signal generated from processing satellite images using CLAS [*Asner et al.*, 2005a, 2006], is critical for an accurate estimation of C budget under a selective logging scenario. Gap fraction affects NPP because it determines the absorbed photosynthetically active radiation, tree functional types within gaps, and light transmitted into gaps. The simulated NPP is also very sensitive to the GOMS parameters, especially in 30–40 years after timber harvest because it determines the radiation available for photosynthesis of the gap species. The fact that the GOMS parameter introduced large uncertainties in the relative sensitivity analyses but not in the absolute sensitivity analysis suggests that the interaction of gap fraction and the GOMS parameters through λ plays an important role in determining the light environment in gaps. Gap fraction and the GOMS parameters combined introduce up to 19% uncertainty to NPP. The maximum light-use efficiency of gap species and meteorological variables also contribute significantly to NPP by modifying APAR or light-use efficiency. The value gap_{th} affects the species composi-

tion in gaps and therefore the NPP in the initial years of regrowth significantly.

[72] Gap fraction and the GOMS parameters also affect respiration because the detrital fractions of wood, leaf, and root carbon pools are tightly correlated with the postlogging gap fraction of each pixel and because the acquired carbon is allocated into different carbon pools and will eventually be turned over for respiration. In the initial 10 years after logging, the decay rates of coarse woody debris, alters the respiration from the ecosystem. Subsequently, heterotrophic respiration is affected because a measurable fraction of initial regrowth turns over rapidly. The uncertainties associated with the GOMS parameters can be as large as 14% by the 40th year of regrowth.

[73] The case presented here for the Tapajos National Forest confirms that selective logging significantly impacts the landscape-level C budget of a forest. Specifically, the damage by logging initially suppresses NPP of the ecosystem by removing a large fraction of foliage. On the other hand, a significant amount of damaged biomass, including leaves, wood, and roots, enters the detrital pools including CWD, which increases the ecosystem heterotrophic respiration for years following timber harvest. Our simulations suggest that logging results in a switch from a forest near steady state to a somewhat large C source. The C source resulting from logging could increase Basin-wide estimates of C losses, compared to current estimates limited to the balance between clear-cut deforestation and regrowth. Our results also show that although the ecosystem returns to a new quasi-steady state for NEP with 20–30 years after timber harvest, both NPP and heterotrophic respiration remain lower than in prelogging conditions. The lower heterotrophic respiration is caused by slower accumulation of biomass in the wood carbon pool due to suppressed NPP levels after logging. Our next step will be to use CASA-3D to quantify Basin-wide carbon fluxes following selective logging to assess the potential impacts of this form of forest use on a broader geographic scale.

Appendix A

[74] Table A1 is a summary of model parameters, their values, and ranges as employed in CASA-3D.

[75] **Acknowledgments.** This study was funded by NASA TEP/LBA grant NNG06GE32A to G. Asner and M. Bustamante.

References

Abuelgasim, A., and A. H. Strahler (1994), Modeling bidirectional radiance measurements collected by the Advanced Solid-State Array Spectroradiometer (ASAS) over Oregon transect conifer forests, *Remote Sens. Environ.*, *47*, 261–275.

Alder, D., and J. N. M. Silva (2000), An empirical cohort model for management of terra firme forests in the Brazilian Amazon, *For. Ecol. Manage.*, *130*, 141–157.

Anderson, M. C., J. M. Norman, T. P. Meyers, and G. R. Diak (2000), An analytical model for estimating canopy transpiration and carbon assimilation fluxes based on canopy light-use efficiency, *Agric. For. Meteorol.*, *101*, 265–289.

Asner, G. P. (1998), Biophysical and biochemical sources of variability in canopy reflectance, *Remote Sens. Environ.*, *64*, 234–253.

Asner, G. P. (2001), Cloud cover in Landsat observations of the Brazilian Amazon, *Int. J. Remote Sens.*, *22*, 3855–3862.

Asner, G. P., C. A. Bateson, J. L. Privette, N. E. Saleous, and C. A. Wessman (1998), Estimating vegetation structural effects on carbon uptake using satellite data fusion and inverse modeling, *J. Geophys. Res.*, *103*(D22), 28,839–28,853.

Asner, G. P., A. R. Townsend, W. Riley, P. A. Matson, J. C. Neff, and C. C. Cleveland (2001), Physical and biogeochemical controls over terrestrial ecosystem responses to nitrogen deposition, *Biogeochemistry*, *54*, 1–39.

Asner, G. P., M. Keller, R. Pereira, and J. Zweede (2002a), Remote sensing of selective logging in Amazonia: Assessing limitations based on detailed field measurements, Landsat ETM+ and textural analysis, *Remote Sens. Environ.*, *80*(3), 483–496.

Asner, G. P., M. Palace, M. Keller, R. Pereira Jr., J. N. M. Silva, and J. C. Zweede (2002b), Estimating canopy structure in an Amazon forest from laser rangefinder and IKONOS satellite observations, *Biotropica*, *34*, 483–492.

Asner, G., M. Keller, R. Pereira, J. Zweede, and J. Silva (2004), Canopy damage and recovery after selective logging in Amazonia: Field and satellite studies, *Ecol. Appl.*, *14*, 280–298.

Asner, G. P., D. E. Knapp, E. N. Broadbent, P. J. C. Oliveira, M. Keller, and J. N. Silva (2005a), Selective logging in the Brazilian Amazon, *Science*, *310*, 480–482.

Asner, G. P., D. E. Knapp, A. N. Cooper, M. M. C. Bustamante, and L. P. Olander (2005b), Ecosystem structure throughout the Brazilian Amazon from Landsat observations and automated spectral unmixing, *Earth Interact.*, *9*(7), EI134, doi:10.1175/EI134.1.

Asner, G. P., E. N. Broadbent, P. J. C. Oliveira, M. Keller, D. E. Knapp, and J. N. M. Silva (2006), Condition and fate of logged forests in the Brazilian Amazon, *Proc. Natl. Acad. Sci. U.S.A.*, *103*(34), 12,947–12,950.

Bossel, H., and H. Krieger (1991), Simulation model of natural tropical forest dynamics, *Ecol. Modell.*, *59*, 37–71.

Botkin, D. B., J. F. Janak, and J. R. Wallis (1972), Some ecological consequences of a computer model of forest growth, *J. Ecol.*, *60*, 849–872.

Brokaw, N. V. (1985), Gap-phase regeneration in a tropical forest, *Ecology*, *66*(3), 682–687.

Brokaw, N. V. L. (1987), Gap-phase regeneration of three pioneer tree species in a tropical forest, *J. Ecol.*, *75*(1), 9–19.

Bugmann, H. (2001), A review of forest gap models, *Clim. Change*, *51*(3–4), 259–305.

Campbell, G. S., and J. M. Norman (1998), *An Introduction to Environmental Biophysics*, 2nd ed., Springer, New York.

Chave, J., et al. (2005), Tree allometry and improved estimation of carbon stocks and balance in tropical forests, *Oecologia*, *145*, 87–99.

Clark, D. A., and D. B. Clark (1999), Assessing the growth of tropical rain forest trees: Issues for forest modeling and management, *Ecol. Appl.*, *9*(3), 981–997.

Clark, D. A., S. Brown, D. W. Kicklighter, J. Q. Chambers, J. R. Thomlinson, J. Ni, and E. A. Holland (2001), Net primary production in tropical forests: An evaluation and synthesis of existing field data, *Ecol. Appl.*, *11*(2), 371–384.

da Rocha, H. R., M. L. Goulden, S. D. Miller, M. C. Menton, L. D. V. O. Pinto, H. C. de Freitas, and A. M. e Silva Figueira (2004), Seasonality of water and heat fluxes over a tropical forest in eastern Amazonia, *Ecol. Appl.*, *14*, S22–S32.

Denslow, J. S. (1987), Tropical rainforest gaps and tree species diversity, *Annu. Rev. Ecol. Syst.*, *18*, 431–451.

Field, C. B., J. T. Randerson, and C. M. Malmstrom (1995), Global net primary production: Combining ecology and remote sensing, *Remote Sens. Environ.*, *51*, 74–88.

Goulden, M. L., S. D. Miller, H. R. da Rocha, M. C. Menton, H. C. de Freitas, A. M. e Silva Figueira, and C. A. Dias de Sousa (2004), Diel and seasonal patterns of tropical forest CO_2 exchange, *Ecol. Appl.*, *14*, S42–S54.

Hirsch, A. I., W. S. Little, R. A. Houghton, N. A. Scott, and J. D. White (2004), The net carbon flux due to deforestation and forest re-growth in the Brazilian Amazon: Analysis using a process-based model, *Global Change Biol.*, *10*(5), 908–924.

Houghton, R. A., D. L. Skole, C. A. Nobre, J. L. Hackler, K. T. Lawrence, and W. H. Chomentowski (2000), Annual fluxes of carbon from deforestation and regrowth in the Brazilian Amazon, *Nature*, *403*, 301–304.

Keller, M., M. Palace, and G. Hurtt (2001), Biomass estimation in the Tapajos National Forest, Brazil: Examination of sampling and allometric uncertainties, *For. Ecol. Manage.*, *154*, 371–382.

Keller, M., et al. (2004a), Ecological research in the large-scale biosphere-atmosphere experiment in Amazonia: Early results, *Ecol. Appl.*, *14*(4), S3–S16.

Keller, M., M. Palace, G. P. Asner, R. Pereira Jr., and J. N. M. Silva (2004b), Coarse woody debris in undisturbed and logged forests in the eastern Brazilian Amazon, *Global Change Biol.*, *10*, 784–795.

King, D. A. (2005), Linking tree form, allocation and growth with an allometrically explicit model, *Ecol. Modell.*, *185*, 77–91.

Lawton, R. O. (1984), Ecological constraints on wood density in a tropical montane rain forest, *Am. J. Bot.*, *71*(2), 261–267.

Li, X., and H. Strahler (1992), Geometric-optical bi-directional reflectance modeling of the discrete crown vegetation canopy: Effect of crown shape

and mutual shadowing, *IEEE Trans. Geosci. Remote. Sens.*, *30*(2), 276–292.

Miller, S. D., M. L. Goulden, M. C. Mento, H. R. da Roch, H. C. de Freitas, A. M. E. S. Figueira, and C. A. D. de Sousa (2004), Biometric and micrometeorological measurements of tropical forest carbon balance, *Ecol. Appl.*, *14*, S114–S126.

Molino, J.-F., and D. Sabatier (2001), Tree diversity in tropical rain forest: A validation of the intermediate disturbance hypothesis, *Science*, *294*, 1702.

Moorcroft, P. R., G. C. Hurtt, and S. W. Pacala (2001), A method for scaling vegetation dynamics: The Ecosystem Demography Model (ED), *Ecol. Monogr.*, *71*(4), 557–586.

Nelson, B. W., R. Mesquita, J. L. G. Pereira, S. G. A. de Souza, G. T. Batista, and L. B. Couto (1999), Allometric regressions for improved estimate of secondary forest biomass in the central Amazon, *For. Ecol. Manage.*, *117*, 149–167.

Nepstad, D. C., et al. (1999), Large-scale impoverishment of Amazonian forests by logging and fire, *Nature*, *398*, 505–508.

Nepstad, D., P. Lefebvre, U. L. Da Silva, J. Tomasella, P. Schlesinger, L. Solorzano, P. Moutinho, D. Ray, and J. G. Benito (2004), Amazon drought and its implication for forest flammability and tree growth: A basin-wide analysis, *Global Change Biol.*, *10*, 704–717.

Olander, L. P., M. M. Bustamante, G. P. Asner, E. Telles, Z. Prado, and P. B. Caramgo (2005), Surface soil changes following selective logging in an eastern Amazon forest, *Earth Interact.*, *9*(4), EI135, doi:10.1175/EI135.1.

Palace, M., M. Keller, G. P. Asner, J. N. M. Silva, and C. Passos (2007), Necromass in undisturbed and logged forests in the Brazilian Amazon, *For. Ecol. Manage.*, *238*, 309–318.

Parton, W. J., C. V. Cole, J. W. B. Stewart, D. S. Ojima, and D. S. Schimel (1989), Simulating regional patterns of soil C, N, and P dynamics in the U.S. central grassland region, in *Ecology of Arable Land*, edited L. Bergström and M. Charholm, pp. 99–108, Springer, New York.

Pereira, R., J. Zweede, G. P. Asner, and M. Keller (2002), Forest canopy damage and recovery in reduced-impact and conventional selective logging in eastern Para, Brazil, *For. Ecol. Manage.*, *168*, 77–89.

Pinard, M. A., and W. P. Cropper (2000), Simulated effects of logging on carbon storage in dipterocarp forest, *J. Appl. Ecol.*, *37*, 267–283.

Potter, C. S., C. B. Field, J. Randerson, P. A. Matson, P. M. Vitousek, and H. A. Mooney (1993a), A model of global net ecosystem production, *Ecol. Soc. Am. Bull.*, *7*(4), 811–841.

Potter, C. S., J. Randerson, C. B. Field, P. A. Matson, P. M. Vitousek, H. A. Mooney, and S. A. Klooster (1993b), Terrestrial ecosystem production: A process model based on global satellite and surface data, *Global Biogeochem. Cycles*, *7*, 811–841.

Randerson, J. T., M. V. Thompson, T. J. Conway, I. Y. Fung, and C. B. Field (1997), The contribution of terrestrial sources and sinks to trends in the seasonal cycle of atmospheric carbon dioxide, *Global Biogeochem. Cycles*, *11*, 535–560.

Risch, A. C., C. Heiri, and H. Bugmann (2005), Simulating structural forest patterns with a forest gap model: A model evaluation, *Ecol. Modell.*, *181*, 161–172.

Saleska, S. R., et al. (2003), Carbon in Amazon forests: Unexpected seasonal fluxes and disturbance-induced losses, *Science*, *302*, 1554–1557.

Shugart, H. H. (1984), *A Theory of Forest Dynamics: The Ecological Implications of Forest Succession Models*, Springer, New York.

Silva, J. N. M., J. O. P. de Carvalho, J. do C. A. Lopes, B. F. de Almeida, D. H. M. Costa, L. C. de Oliveira, J. K. Vanclay, and J. P. Skovsgaard (1995), Growth and yield of a tropical rain forest in the Brazilian Amazon 13 years after logging, *For. Ecol. Manage.*, *71*, 267–274.

Silver, W., J. C. Neff, M. McGroddy, E. Veldkamp, M. Keller, and R. C. Oliveira Jr. (2000), Effects of soil texture on belowground carbon and nutrient storage in a lowland Amazonian forest ecosystem, *Ecosystems*, *3*, 193–209.

Spitters, C. J. T., H. A. J. M. Toussaint, and J. Goudriaan (1986), Separating the diffuse and direct component of global radiation and its implications for modeling canopy photosynthesis, Part I. components of incoming radiation, *Agric. For. Meteorol.*, *38*, 217–229.

Sposito, T., and F. A. M. Santos (2001), Scaling of stem and crown in eight *Cecropia* (Cecropiaceae) species of Brazil, *Am. J. Bot.*, *88*(5), 939–949.

Swaine, M. D., and T. C. Whitmore (1988), On the definition of ecological species groups in tropical rain forests, *Vegetatio*, *75*, 81–86.

Vieira, S., S. Trumbore, P. B. Camargo, D. Selhorst, J. Q. Chambers, N. Higuchi, and L. A. Martinelli (2005), Slow growth rates of Amazonian trees, *Proc. Natl. Acad. Sci. U.S.A.*, *102*(51), 18,502–18,507.

Webb, E. L. (1998), Gap-phase regeneration in selectively logged lowland swamp forest, northeastern Costa Rica, *J. Trop. Ecol.*, *14*, 247–260.

Whitemore, T. C. (1998), *An Introduction to Tropical Rain Forests*, 2nd ed., Clarendon, Oxford, U.K.

G. P. Asner, J. A. Berry, and M. Huang, Department of Global Ecology, Carnegie Institution of Washington, Stanford, CA 94305, USA. (mhuang@globalecology.stanford.edu)

M. Keller, USDA Forest Service, International Institute of Tropical Forestry, Rio Piedras, PR 00928-5000.